Satellite Detection of NO_2 Distributions Using TROPOMI and TEMPO and Comparison with Ground-Based Concentrations

Summer Acker,[1] Tracey Holloway[1, 2] and Monica Harkey[1]

[1] Nelson Institute Center for Sustainability and the Global Environment, University of Wisconsin-Madison, Madison, WI 53705, United States of America

[2] Department of Atmospheric and Oceanic Sciences, University of Wisconsin-Madison, Madison, WI 53705, United States of America

Correspondence to: Tracey Holloway (taholloway@wisc.edu)

Abstract

In this study we assess the capability of current-generation satellites to capture the variability of near-surface nitrogen dioxide (NO_2) monitoring data, with the goal of supporting health and regulatory applications. We consider NO_2 vertical column densities (VCD) over the United States from two satellite instruments, the Tropospheric Monitoring Instrument (TROPOMI), and Tropospheric Emissions: Monitoring of Pollution (TEMPO), and compare with ground-based concentrations as measured by the EPA's Air Quality System (AQS) monitors. While TROPOMI provides a longer-term record of assessment (2019-2023), TEMPO informs diurnal patterns relevant to evaluating peak NO_2. We analyze frequency distributions and quantify their similarity using the Jensen-Shannon Divergence (JSD), where smaller values indicate better agreement. Satellite and ground monitor NO_2 distributions are most similar at non-roadway monitors (JSD = 0.008) and are most different at interstate (JSD = 0.158) and highway (JSD = 0.095) monitors. Seasonal analysis shows the most similarity in distributions in winter (JSD = 0.010), and the most difference in summer (JSD = 0.035). Across seasons and monitor locations, the calculated 1:30 pm LT TEMPO consistently exhibits better or comparable JSDs to TROPOMI (TEMPO: 0.005 to 0.151; TROPOMI: 0.012 to 0.265). TEMPO's agreement with monitors in both December 2023 and July 2024 is found to be best around midday, with non-road monitors in July having the best alignment (JSD = 0.008) at 16 UTC (~11 am LT). These

findings highlight the ability of TROPOMI and TEMPO to complement existing ground-based monitors, and demonstrate their potential for monitor siting, regulatory, and public health applications.

1 Introduction

Nitrogen dioxide (NO_2) is a gas released through high temperature combustion processes such as the burning of fossil fuels (Lee et al., 1997; Richter et al., 2005), with on-road vehicles, power plants, and industrial processes representing the largest anthropogenic sources in the United States (U.S.; van der A et al., 2008) as well as lightning NO_X emissions (Dang et al., 2023) and soil microbial activity (Huber et al., 2020) from natural sources. Exposure to elevated levels of NO_2 has been linked to respiratory and cardiovascular diseases (Mills et al., 2015; Urbanowicz et al., 2023; Meng et al., 2021), especially asthma in children (Mölter et al., 2014; Anenberg et al., 2022; Achakulwisut et al., 2019), as well as premature mortality (Camilleri et al., 2023; Hales et al., 2021; Huangfu and Atkinson, 2020), and other diseases (Xia et al., 2024; Bai et al., 2018). NO_2 plays a critical role in the formation of ozone, which also causes respiratory health problems and is harmful to ecosystems (Grulke & Heath, 2019; Sillman, 1999). It is also a precursor to nitrate (Behera & Sharma, 2012), a type of fine particulate matter ($PM_{2.5}$), which can penetrate deep into the lungs and exacerbate respiratory and heart conditions (Sangkham et al., 2024; Sharma et al., 2020), as well as cause premature death (Orellano et al., 2020; Thangavel et al., 2022).

Due to its radiative characteristics, NO_2 may be observed by satellites during daylight hours (Boersma et al., 2018; Van Geffen et al., 2020; Veefkind et al., 2012), and NO_2 has emerged as one of the most air-quality-relevant pollutants from satellites (Holloway et al., 2021). Several studies have highlighted the potential for satellite NO_2 data to supplement ground-based networks to support health analysis and air quality management (Duncan et al., 2014; Lee & Koutrakis, 2014). The 2017 launch of the Tropospheric Monitoring Instrument (TROPOMI; Boersma et al., 2018; Van Geffen et al., 2020; Veefkind et al., 2012) advanced these applications (Goldberg et al., 2021; Griffin et al., 2019; Kim et al., 2024; Yu & Li, 2022; Dressel et al., 2022; Goldberg et al., 2024; H. J. Lee et al., 2023). The Tropospheric Emissions: Monitoring of Pollution (TEMPO; Chance et al., 2019; Naeger et al., 2021; Zoogman et al., 2017) provides

59 further advancements with daytime hourly observations of NO_2 over North America and finer
60 spatial coverage.

61 While advanced methods exist to calculate near-surface NO_2 from satellite columns (Ahmad et
62 al., 2024; Kim et al., 2021; Shetty et al., 2024; Virta et al., 2023), there is also a strong interest in
63 the utilization of satellite vertical column density (VCD) to directly infer NO_2 concentrations
64 analogous to ground-based monitors (Kim et al., 2024; Lamsal et al., 2014; Griffin et al., 2019;
65 Yu & Li, 2022; Zhang et al., 2018; Lamsal et al., 2015; Goldberg et al., 2021; Dressel et al.,
66 2022; Goldberg et al., 2024; Harkey & Holloway, 2024; Bechle et al., 2013; H. J. Lee et al.,
67 2023; Xu & Xiang, 2023). This study extends prior assessments of NO_2 column-to-surface
68 agreement, where we focus on frequency distributions to capture the net impact of day-to-day
69 variability.

70 The relationship between surface NO_2 and column abundance is influenced by physical and
71 chemical processes, many of which have seasonal components. In winter, shallow boundary
72 layers trap pollutants near the surface, leading to higher surface concentrations and increasing
73 surface-to-column agreement (Harkey et al., 2015). In summer, higher temperatures and
74 increased sunlight accelerate photochemical reactions, converting NO_2 into ozone and other
75 secondary pollutants, and decreasing surface-to-column agreement (Boersma et al., 2009).
76 Seasonal changes in emissions, such as high building-heating emissions in winter, and high
77 power plant emissions in summer (Frost et al., 2006; Levinson & Akbari, 2010) interact with
78 atmospheric processes causing an increase in NO_2 column abundance in winter in four-season
79 climates (Shah et al., 2020). Processes affecting the sources and sinks of NO_2 at the surface and
80 through the vertical column can also lead to temporal lags, with peak surface NO_2 preceding
81 peak column NO_2 in the mornings (Harkey et al. 2024).

82 Frequency distributions capture the variability, extremes, and patterns of pollutant abundance,
83 relevant to air quality standards, pollution trends, and the effectiveness of emission control
84 measures (Knox and Lange, 1974; Pollack, 1975; Venkatram, 1979; Chowdhury et al., 2021;
85 Mondal et al., 2021). For example, Mondal et al. (2021) used frequency distributions of ground-
86 based monitors to examine changes in air quality across Delhi and Kolkata during COVID-19
87 lockdown phases, showing how reduced human activity led to shifts in pollutant levels. We

extend this line of analysis by comparing NO_2 distributions across multiple dimensions with TROPOMI and include time-of-day and resolution-dependence of results using data from TEMPO.

In this work, we consider: (1) How do the distributions of satellite NO_2 VCD compare with those for near-surface NO_2? (2) To what degree does new hourly data from TEMPO improve the agreement between surface and space based NO_2 distributions? For both questions, we consider spatial variability, especially proximity to roadways, and temporal variability including seasonality and diurnal variability. By considering the ability of satellites to capture peak NO_2 values in a comparable distribution to surface data, we consider how satellite VCDs can support air quality management, improve health impact analysis, and inform air pollution monitor siting.

2 Data and Methods

In this study, we evaluate the ability of two satellite instruments, TROPOMI and TEMPO, to capture the spatial and temporal variability in NO_2 surface concentration distributions across the continental United States (CONUS), as measured by AQS monitors. By comparing the coefficient of variation (CV) and Jensen-Shannon divergence (JSD) between satellite and monitor data, we aim to assess the alignment between the datasets.

2.1 EPA Surface Monitor Data

The Environmental Protection Agency (EPA) Air Quality System (AQS) contains hourly NO_2 measurements from ground-based monitors, providing high temporal resolution data that are critical for assessing compliance with the U.S. National Ambient Air Quality Standards (NAAQS). There are two NAAQS related to NO_2: one for annual average concentration, set at 53 ppb, and one based on peak 1-hour concentrations, set at 100 ppb, based on the 3-year average of the 98^{th} percentile of the yearly distribution of 1-hour daily maximum NO_2 concentrations (EPA, 2010). Enforcement of these standards relies on data from AQS NO_2 monitors, a network that includes 431 monitors as of August 2024. Because NO_2 has a relatively short atmospheric lifetime, typically ranging from a few hours to a day depending on meteorological conditions (Lange et al., 2022; Liu et al., 2021), ground monitors are expected to capture local conditions (Wang et al., 2020).

The EPA AQS data (EPA, 2025) was used to access NO_2 monitor data for the years 2019 through 2023 from all available sites in CONUS during this time period (503 unique monitors from 2019 to 2023). We note that there are some areas that are overrepresented by NO_2 monitors, and others that are lacking monitors. Specifically, most monitors are located in urban areas, especially on the East Coast and in Southern California, meaning that rural areas tend to be less represented by ground monitors (Kerr et al., 2023). Most monitors use a chemiluminescence method, where the amount of NO_2 that is converted to NO is measured by a molybdenum oxide converter (Fontijn et al., 1970). The converter also reacts with other oxidized nitrogen compounds such as nitric acid (HNO_3) and peroxyacetyl nitrate (PAN) to form NO (Dunlea et al., 2007; Steinbacher et al., 2007), which can lead to an overestimation of NO_2. Corrections for this bias have been applied when comparing with satellite observations (e.g. Cooper et al., 2020; Lamsal et al., 2015; Li et al., 2021). Uncorrected AQS NO_2 has been used for determining compliance with the NAAQS and for health assessments, which is the approach we take here, consistent with prior studies focused on regulatory relevance (Novotny et al., 2011; Penn & Holloway, 2020; Harkey and Holloway, 2024; Goldberg et al., 2021; Kim et al., 2024; Duncan et al., 2013; Qin et al., 2019). More recently, some NO_2 monitors have been added to the network which measure "true NO_2" using Cavity Attenuated Phase Shift Spectroscopy (CAPS, Kebabian et al., 2005). These monitors are expected to be more representative of ground-level NO_2 concentrations and should have less overestimations since they directly measure NO_2 and no other species (Ge et al., 2013). Some of the monitors used in this study use CAPS methodology to measure NO_2. We discuss the comparison of CAPS versus traditional NO_2 monitors in results Sect. 3.1.

Hourly AQS measurements at 13:00 and 14:00 local time (LT) were averaged to align with the TROPOMI overpass of ~13:30 LST. Hourly AQS measurements from 12:00 GMT to 23:00 GMT are compared with hourly TEMPO data for daylight hours. For both the TROPOMI and TEMPO analyses, AQS data are filtered to ensure consistency with satellite data availability. As a result of filtering monitoring data for TROPOMI and TEMPO separately, the subsets of monitor data available for comparison with each instrument differ, even for the same time periods.

2.2 TROPOMI Data

The Tropospheric Monitoring Instrument (TROPOMI; European Space Agency, 2021) is on board the Copernicus Sentinel-5 Precursor satellite which has a daily, local overpass time of ~13:30 LST (Veefkind et al., 2012). Currently, the highest resolution of TROPOMI is 3.5 km by 5.5 km at nadir which has increased from 3.5 km by 7.0 km since August 6th, 2019. Daily TROPOMI NO_2 data for the years 2019 through 2023 were allocated to a 4 km x 4 km grid over CONUS using the Wisconsin Horizontal Interpolation Program for Satellites (WHIPS; Center for Sustainability and the Global Environment, 2024; Harkey et al., 2015, 2021; Harkey and Holloway, 2024; Penn and Holloway, 2020). Using WHIPS, we also remove data with a quality flag lower than 0.75. Each monitor location was compared with the 4 km x 4 km gridded TROPOMI value in the corresponding grid cell. December 2023 and July 2024 4 km x 4 km TROPOMI NO_2 data were also collected for each of the monitors for comparison with TEMPO data.

A 4 km x 4 km oversampled grid is used as opposed to the 1 km x 1 km oversampled grid since this study focuses on daily observations, and the 1 km x 1 km grid is best suited for monthly or annual averages (Goldberg et al., 2021). To ensure a valid number of TROPOMI pixels were being represented despite the higher grid resolution, we analyzed the number of ground monitors falling within each TROPOMI pixel by performing a spatial join between ground monitor locations and the oversampled 4 km x 4 km TROPOMI grid. About 97% of TROPOMI pixels contain only one monitor, with only a small number of pixels (2.7%) containing more than one. Figure S1 shows the number of monitors per TROPOMI pixel (locations where there are more than 1 monitor per TROPOMI pixel) and the number of valid TROPOMI retrievals from 2019 to 2023 at each grid cell, confirming that monitors are well-distributed enough to not disproportionately cluster within a small subset of satellite pixels. Since monitors are spread across the entire U.S. and most are at least 4 km apart, there is generally sufficient separation to ensure that most monitors are assigned to distinct TROPOMI pixels rather than falling into the same grid cells repeatedly.

2.3 TEMPO Data

The TEMPO instrument launched onboard the Intelsat 40e mission (NASA, 2024), a geostationary satellite, on April 7, 2023. TEMPO provides hourly measurements of atmospheric

pollutants over North America (Chance et al., 2019; Naeger et al., 2021; Zoogman et al., 2017). TEMPO achieves a spatial resolution of approximately 2.1 km in the north-south direction and 4.5 km in the east-west direction at the center of its Field of Regard (FOR), centered around 36.5° N and 100° W (Chance et al., 2019). The TEMPO Level-3 (L3) NO_2 data (Suleiman, 2024) used in this study were accessed through NASA's EarthData Search portal.

In order to synchronize TEMPO and ground-based hourly measurements, TEMPO timestamps were rounded to the nearest hour, with mid-hour values rounded up. All files within each rounded-hour group were averaged, producing a single NO_2 value per hour per day. Only TEMPO observations with a main data quality flag of 0 and cloud fraction at or less than 0.2 were retained, in line with TEMPO documentation guidelines (NASA Langley Research Center, 2024).

For the comparison with TROPOMI, the UTC equivalents of 1 pm and 2 pm LT were determined for each time zone based on the latitude and longitude of each monitor location. TEMPO NO_2 values corresponding to these calculated UTC hours were averaged to align with the TROPOMI overpass time (~13:30 LST). Similarly, for ground-based measurements, the monitor data were filtered to include only values corresponding to 1 pm and 2 pm LT and then averaged.

2.4 Monitor Classification

To classify the monitors by roadway proximity, the state-level Census Bureau's 2021 TIGER/Line shapefiles for Primary and Secondary Roads (2021 TIGER/Line® Shapefiles, 2025) were combined to form a comprehensive dataset for the CONUS domain.

To evaluate how TROPOMI and ground-based monitor NO_2 values vary by proximity to a road, monitors were also assigned to different groups based on their distance from a road (≤20-m, 20 to 50-m, 50 to 300-m, 300-m to 1 km, and > 1 km), where buffer distances are calculated from the road shapefiles (Figure S3). There were 9 monitors that were 20 meters or less away from a road, 66 between 20 and 50 meters from a road, 108 between 50 and 300 meters, 167 between 300 meters and 1 kilometer, and 153 that were greater than 1 kilometer from a road.

Roads were also classified into three categories: (1) interstates, (2) highways, and (3) other roads, based on their route type code (RTTYP) values. Where monitors are considered as representing a roadway category, we followed the criteria of the EPA Near-Road-Network (Gantt et al., 2021; Kim et al., 2024) to merge monitor locations with road buffers, considering the 50-m buffer recommended by the EPA, as well as a less restrictive 300-m buffer. In each case, monitors inside the buffer of a particular roadway type were classified as representing that category. If a monitor fell within multiple buffers, it was assigned the classification of the largest road type. Monitors not falling within any buffers were classified as "non-roadway."

Using the 50-m buffer, 58 monitors were classified as “interstate,” 17 as “highway,” and 428 as “non-roadway” (Figure S2; no monitors classified as “other roads”). Using the 300-m buffer, 91 monitors were classified as “interstate,” 90 as “highway,” 320 as “non-roadway,” and 2 as “other roads.” Since there were no monitors classified as “other roads” for the 50-m buffer, this category is excluded from the analysis.

We classified interstate monitors as urban or rural using the U.S. Census Bureau 2020 Urban Areas Tiger/Line Shapefile (U.S. 2020 Urban Areas Shapefile, 2025). Only one interstate monitor was identified as rural, so this analysis is not included.

2.5 Data Analysis

The coefficient of variation (CV) was calculated for ground-level monitor data and for satellite data. This metric was used to compare the relative variability of NO_2 between satellite and ground-level data despite different measurement units (Aerts et al., 2015). CV is defined as the ratio of the standard deviation (σ) to the mean (μ) of the data:

$$CV = \left(\frac{\sigma}{\mu}\right) \times 100$$

The Jensen-Shannon Divergence (JSD) is used to quantify the similarity between the distributions of NO_2 from the satellite and ground-level monitors despite the different measurement units (Menéndez et al., 1997). The JSD is a robust metric for comparing probability distributions that is used within a wide variety of fields, including machine learning

(Thiagarajan & Ghosh, 2024; Saurette et al., 2023; Tsigalou et al., 2021; Melville et al., 2005), data science (Toledo et al., 2022; Zhao et al., 2024), biology (Yan et al., 2021; Jones et al., 2023; Ahmed et al., 2023), and meteorology (Kibirige et al., 2023). In environmental research using satellite data, the JSD has shown that the Mangrove Forest Index (MFI) from Sentinel-2 imagery outperforms traditional vegetation indices in distinguishing submerged mangrove forests (Jia et al., 2019). In air quality, the JSD has been used to compare modeled and measured $PM_{2.5}$ (Yang et al., 2024), and to compare an air quality index (AQI) with measurements of specific air pollutants (Wang & Zhang, 2022).

To calculate the JSD, each dataset was binned, with a bin size of 1 ppb (for ground monitors) or 1 x 10^{15} molecules/cm^2 (for satellite data), ranging from 0 to 40 ppb or 40 x 10^{15} molecule/cm^2, with an additional bin for values exceeding 40 ppb or 40 x 10^{15} molecule/cm^2. For visualization purposes, the frequency distributions are binned with the ground monitors ranging from 0 to 40 ppb and the satellite data ranging from 0 to 30 x 10^{15} molecule/cm^2, with an additional bin for values exceeding 40 ppb or 30 x 10^{15} molecule/cm^2. Depending on the specific analysis, NO_2 data are grouped by: (1) Distance from roadways (in meters) – TROPOMI daily data from 2019 to 2023 (and corresponding ground monitors) are grouped by proximity to roads to assess spatial alignment; (2) season – TROPOMI daily data from 2019 to 2023 (and corresponding ground monitors) are grouped by season to analyze temporal alignment; (3) month – TROPOMI daily data from December 2023 and July 2024, along with TEMPO and ground monitors at the TROPOMI overpass time (~1:30 pm LT, represented by the average of 1 pm and 2 pm LT data), are grouped by month to compare the temporal differences in alignment between TEMPO and TROPOMI; and (4) road type (interstate, highway, non-roadway) – Both TROPOMI (daily), TEMPO (calculated overpass time and hourly), and ground monitor data are grouped by road type to evaluate varying alignment based on road classifications.

Binned data were then normalized to form probability distributions. The divergence was calculated as:

$$JSD(P,Q) = \frac{1}{2}[D_{KL}(P||M) + D_{KL}(Q||M)]$$

where P and Q represent the probability distributions from the monitor and satellite data, respectively, and M is the average of P and Q. The divergence D_{KL} is the Kullback-Leibler divergence between each distribution and their mean (Clim et al., 2018). JSD values range from 0 to 1, with lower values indicating greater similarity between the satellite and monitor distributions. In general, a JSD < 0.1 indicates very good alignment, 0.1 ≤ JSD < 0.3 indicates moderate alignment, and JSD ≥ 0.3 (Kibirige et al., 2023) indicates poor alignment.

3 Results

To evaluate the agreement between satellite and monitored NO_2 distributions, we consider the impact of monitor location using TROPOMI; impact of season using TROPOMI; the comparison of distributions between TROPOMI and TEMPO; and the impact of time-of-day using TEMPO.

3.1 Alignment of TROPOMI NO_2 Distributions with Surface NO_2 Distributions

This section analyzes TROPOMI and ground-based NO_2 measurements across varying distances from roads, different seasons, and at monitors located near interstates, highways, and non-roadway sites. Our results show that as the distance from roads increases, the distributions of surface and column NO_2 become more similar. Monitor distributions near interstates and highways exhibit lower agreement with TROPOMI distributions compared to those farther from major roadways. Seasonally, alignment is strongest in winter and weakest in summer.

Figure 1 illustrates the distribution of NO_2 levels measured by AQS ground-based monitors and TROPOMI observations as a function of distance from roadways using daily measurements from 2019 to 2023. For both data sources, mean, peak, and minimum NO_2 are all highest in the 20 – 50 m distance category (the second closest near-road category). NO_2 abundance decreases as distance-to-road increases, and to a lesser extent as distance-to-road decreases. The somewhat lower abundance in the ≤ 20 m category vs. the 20 – 50 m category may be due to the speciation of NO_X, where nitric oxide (NO) is more abundant and converts to a higher fraction of NO_2 as distance-to-road increases (Kimbrough et al., 2017). Most direct vehicle emissions are in the form of NO, and close to the roadway, NO and NO_2 readily convert between forms. Limited ozone availability—especially during stable conditions, which contribute to suppressed vertical mixing—can slow the conversion of NO to NO_2 (Richmond-Bryant et al., 2017). As a result, NO_2 may initially be suppressed very close to the road, and changes in total NO_X are primarily

driven by mixing and dilution rather than chemical transformation. NO_2 peaks in the 20–50 m range likely because this zone allows for sufficient time and space for NO to oxidize to NO_2 while still being close enough to the emission source to experience elevated concentrations; beyond this range, concentrations decrease with distance due to dispersion and dilution of pollutants into the surrounding atmosphere. Mean monitored NO_2 is 6.85 ppb at ≤ 20 m, 10.47 ppb at 20 – 50 m, 4.53 ppb at 50 – 300 m, 3.71 ppb at 300 m – 1 km, and 2.80 ppb at > 1 km. Mean TROPOMI NO_2 is 3.38 x 10^{15} molecules/cm^2 at ≤ 20 m, 4.21 10^{15} molecules/cm^2 at 20 – 50 m, 3.00 x 10^{15} molecules/cm^2 at 50 – 300 m, 3.72 x 10^{15} molecules/cm^2 at 300 m – 1 km, and 3.13 x 10^{15} molecules/cm^2 at > 1 km. Monitor values show a higher sensitivity to roadway proximity, where the highest mean monitored concentration is 375% of the lowest mean concentration, compared to TROPOMI where the highest mean VCD is 140% of the lowest mean VCD.

Monitored NO_2 levels drop over 50% at ~50 m from the roadway (based on change in the mean, upper 2.5 interquartile range, IQR, and the upper 1.5 IQR), a finding that compares with a 31% reduction in NO_2 between 20m and 300m from Kimbrough et al. (2017), as well as other studies that identify a decrease in NO_2 at further distances (Karner et al., 2010; Richmond-Bryant et al., 2017). TROPOMI VCDs also show the greatest change with roadway distance at ~50 km, but by less than 30% (based on change in the mean, upper 2.5 IQR, and the upper 1.5 IQR).

Just as total NO_2 abundance, from both monitors and satellite, is highest at distances of 20-50 m from the roadway, the range of daily values is also widest for the 20 – 50 m range and smallest at the > 1 km range. Monitored values have a standard deviation of 8.24 ppb in the 20 – 50 m range, and a standard deviation of 3.39 ppb in the > 1 km range. The distribution of satellite data does not vary as much in size across roadway locations, with a standard deviation of 3.90 x 10^{15} molecules/cm^2 for the 20 – 50 m range and 3.31 x 10^{15} molecules/cm^2 for the > 1 km range. In the 20 – 50 m range, the upper IQR of AQS NO_2 is 38% higher than the mean. TROPOMI shows less variability than the monitors, with the 20 – 50 m upper IQR 16% higher than the mean. As distance from the roadway increases, the distributions of data from the ground and satellite become more comparable. In the > 1 km range, the upper IQR of monitor NO_2 is 23% higher than the mean and the upper IQR of satellite data is 15% higher than the mean. The ranges show more similarity at greater distances from the roadway, but even at distances of > 1 km, the range

of monitored values exceeds the range of satellite VCDs. These patterns agree with Kim et al. (2024), who found that surface monitors show better agreement with TROPOMI further from major roads. This improved alignment at greater distances likely reflects the reduced influence of localized emission sources, which tend to create sharp gradients and rapid variability near roads. In areas further from traffic, NO_2 concentrations vary more gradually or are generally more uniform. As a result, surface monitors away from roads reflect broader conditions, in better agreement with the coarser spatial resolution of TROPOMI.

When analyzed by season (Figure S4), the relationships are similar, except winter shows the highest IQRs, with the 20 to 50 m distance group having an IQR of 11.40 ppb for monitors and 4.96 x 10^{15} molecules/cm^2 for TROPOMI, and summer, the lowest IQRs for both monitors (IQR = 9.05 ppb) and TROPOMI (IQR = 1.71 x 10^{15} molecules/cm^2). In the greater than 1 km distance group, again winter has the highest IQRs (monitor IQR = 4.60 ppb; TROPOMI IQR = 3.95 x 10^{15} molecules/cm^2) and summer the lowest IQRs (monitor IQR = 2.05 ppb; TROPOMI IQR = 1.55 x 10^{15} molecules/cm^2).

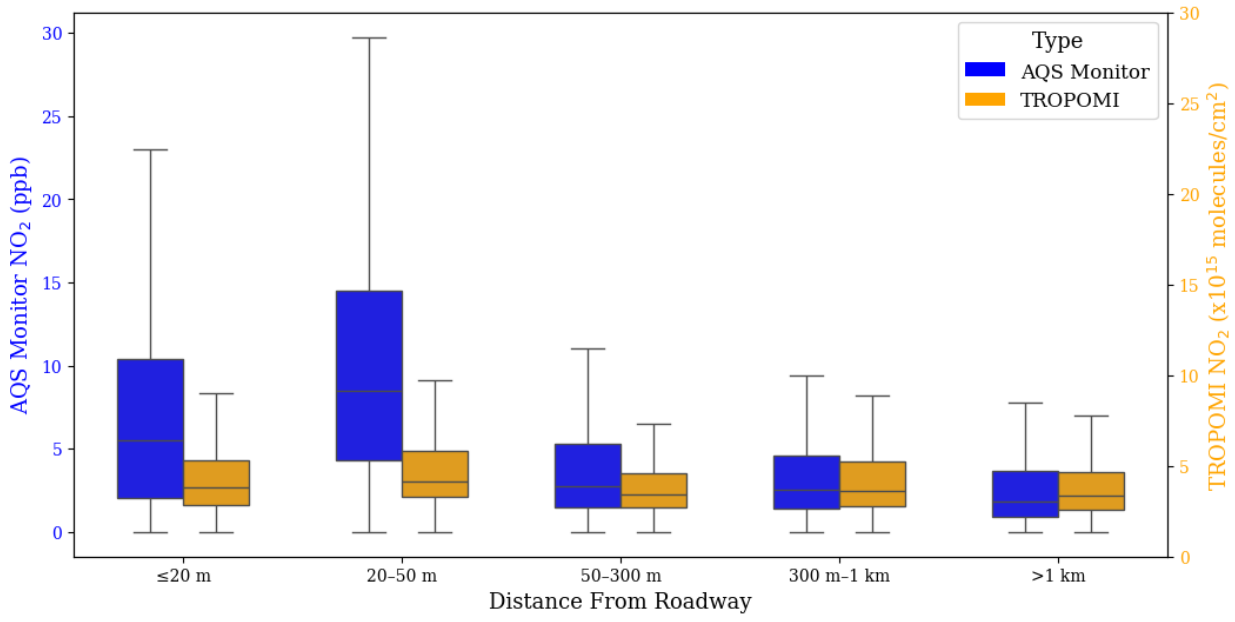

Figure 1. Box plots show median and interquartile ranges of all daily 2019 to 2023 NO_2 as measured by AQS monitors (blue) and TROPOMI (orange) across various distances from roadways, with the whiskers extending to the 1.5 IQR range. No outliers are shown. The left y-

axis represents AQS monitor values in parts per billion (ppb), and the right y-axis represents TROPOMI NO_2 values in 10^{15} molecules per cm^2. The distance categories from the roadway include ≤ 20 m, 20-50 m, 50-300 m, 300 m-1 km, and > 1 km.

To consider the shape of monitored and satellite NO_2 distributions, we consider the effect of season in Fig. 2. The winter distributions (Figure 2a, calculated from December, January, and February data) exhibit the longest tails and highest NO_2 values. In winter, the 90th percentile of monitoring data is 14.80 ppb and the 90th percentile of TROPOMI data is 10.93 x 10^{15} molecules/cm^2. Spring distributions (Figure 2b; March, April, and May) show intermediate behavior, with lower values and shorter tails than winter and fall, but higher than summer (90th percentile from monitors = 9.71 ppb; 90th percentile from TROPOMI = 6.19 x 10^{15} molecules/cm^2). In summer (Figure 2c, June, July, and August), the distributions exhibit the shortest tails, and the lowest NO_2 values (90th percentile from monitors = 9.00 ppb; 90th percentile from TROPOMI = 4.57 x 10^{15} molecules/cm^2). Fall (Figure 2d; September, October, and November) also shows intermediate behavior, generally between winter and spring (90th percentile from monitors = 12.15 ppb; 90th percentile from TROPOMI = 7.44 x 10^{15} molecules/cm^2). The higher NO_2 values in winter from monitor and TROPOMI data are attributed to reduced photochemical activity in winter leading to longer NO_2 lifetimes (Harkey et al., 2015; Boersma et al., 2009; Shah et al., 2020).

The highest percent frequencies for the monitor and TROPOMI distributions generally occur within the 1–2 ppb or 1–2 x 10^{15} molecules/cm^2 bin. However, the winter TROPOMI distribution peaks in the 2–3 x 10^{15} molecules/cm^2 bin with a percent frequency of 18.14%, compared with winter monitor highest frequency of 14.33%. The highest percent frequency in spring from TROPOMI is 30.39% versus monitor 24.15%; in summer TROPOMI is 34.35% versus monitor of 24.68%; in fall TROPOMI is 24.90% versus monitor of 18.89%. These results indicate that TROPOMI consistently records higher peak frequencies than the monitors, whereas monitors consistently show a wider distribution.

Figure 2 provides a seasonal breakdown of the coefficient of variation (CV) and Jensen-Shannon divergence (JSD) for both monitor and TROPOMI data across all monitors. Summer exhibits the highest variability in monitored NO_2 concentrations (CV = 127.99%), but the lowest variability in satellite observations (CV = 78.00%). The highest variability in TROPOMI occurs in winter

(CV = 103.51%), similar to the variability from monitor data (CV = 104.48%). Satellite CVs generally follow a similar pattern to that of monitors, though the overall variability is lower for satellite data across seasons.

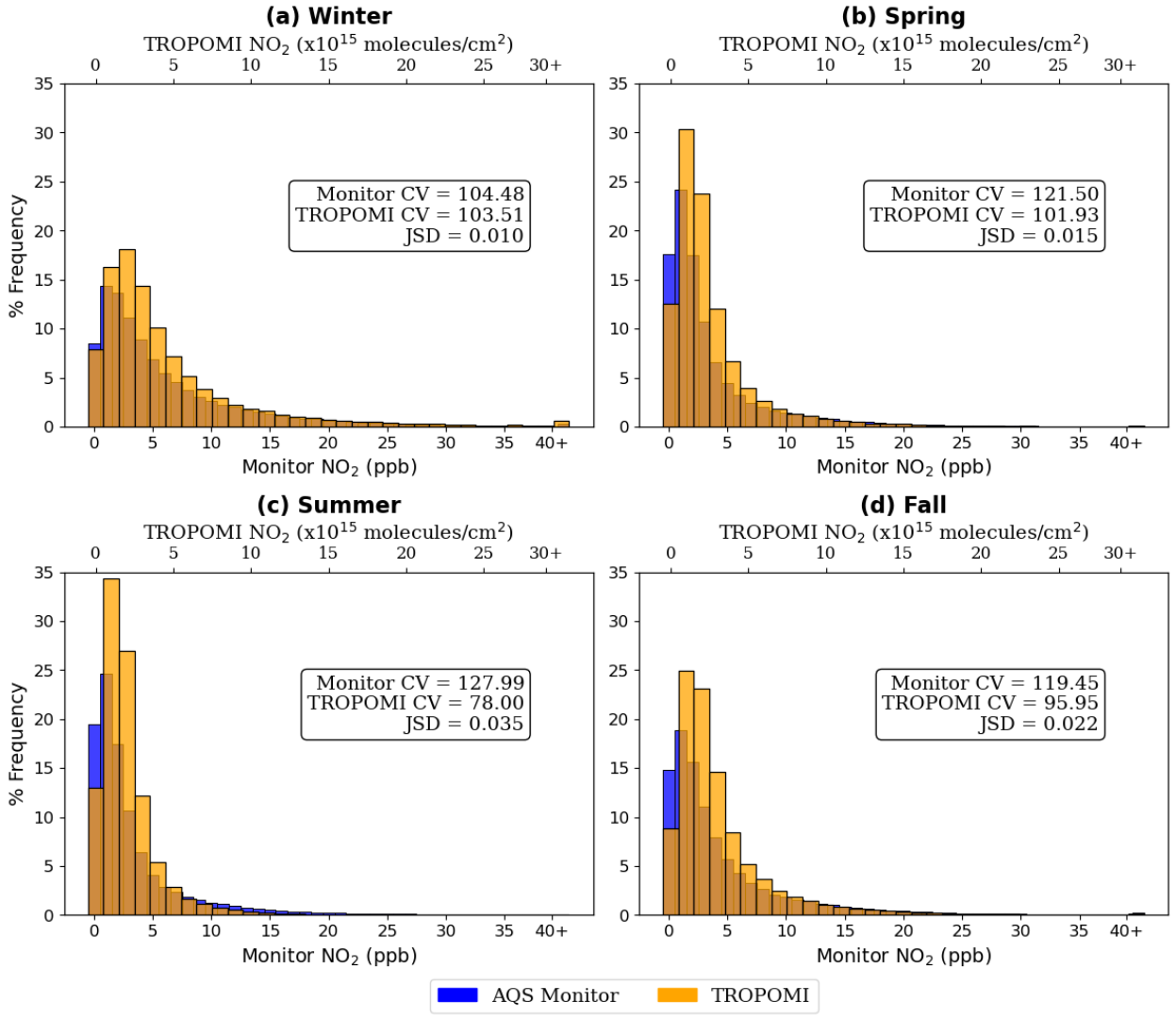

Figure 2. Seasonal frequency distributions of 2019-2023 NO_2 as measured by AQS ground-based monitors (blue) and TROPOMI (light orange) data for four seasons: a) winter, b) spring, c) summer, and c) fall. The x-axes indicate the range of NO_2, with the primary, lower x-axis showing monitor NO_2 concentrations in parts per billion (ppb) and the secondary, upper x-axis showing TROPOMI NO_2 VCD in 10^{15} molecules per cm^2. The boxes show the Coefficient of Variation (CV; %) and Jensen Shannon Divergence (JSD) for each season.

This reduced variability in satellite observations can likely be attributed to the vertical mixing reflected in satellite retrievals, as well as horizontal spatial averaging reflected in satellite data versus point-based NO_2 that are captured by ground monitors. This finding is consistent with previous studies that highlight the spatial averaging nature of satellite-based measurements, which integrate NO_2 amounts over a larger area than the point-based monitors (Ialongo et al., 2020).

Across all seasons shown in Fig. 2, JSD values are all low (< 0.1), indicating that TROPOMI may be good at predicting surface NO_2 across seasons. The alignment is strongest in winter (JSD = 0.010), while the divergence is highest in summer (JSD = 0.035), meaning the monitors and TROPOMI align best when the NO_2 lifetime is long in the colder months, and they align the worst when the NO_2 lifetime is short in the warmer months. The better alignment in winter could also be attributed to winter having the largest range of values in the data, which reduces the sensitivity of the JSD calculation to small differences in the distributions. A wider spread in NO_2 values means that relative discrepancies between TROPOMI and monitor measurements are smaller in proportion to the total variability, potentially leading to greater similarity.

Across seasons, we find that CAPS or "true NO_2" monitors tend to have slightly worse alignment with TROPOMI than traditional, chemiluminescence monitors. Out of the monitors used in this study, 102 were identified as CAPS monitors, and 401 as traditional monitors. In winter, CAPS monitors have a JSD of 0.027 and traditional monitors a JSD of 0.009. In summer, CAPS monitors have a JSD of 0.078 and traditional monitors a JSD of 0.03. With all seasons combined, CAPS monitors have a JSD of 0.047 and traditional monitors have a JSD of 0.016.

Table 1 shows the CV and JSD for both monitor and satellite data from 2019 through 2023, aggregated across all seasons and separated by monitor classification (interstate, highway, and non-roadway), where roadway monitors are classified as being within 50 meters (Table 1a) or 300 meters (Table 1b) of a road. For the 50-m buffer (Table 1a), the coefficient of variation for ground-based monitor data increases progressively from interstate monitor locations to non-roadway locations, with interstate monitors exhibiting the lowest variability (CV = 75.07%) and non-roadway monitors showing the highest variability (CV = 118.17%). This indicates that NO_2 concentrations measured by ground monitors in interstate areas are more consistent compared to non-roadway regions. This pattern is mirrored in the satellite data, with CV values ranging from

91.62% for highway monitors to 106.16% for non-roadway monitors. These patterns suggest that regular emissions play a larger role in determining near-road NO_2, where non-road areas vary with changes in wind patterns and the chemical environment.

For highway monitors, the CVs of satellite (CV = 91.62%) and monitor data (CV = 96.27%) are similar, indicating that TROPOMI performs similarly to ground monitors in capturing NO_2 variability along highways. Near interstates, TROPOMI (CV = 92.60%) may capture more variability than the ground-based measurements (CV = 75.07%), a finding that contrasts with Fig. 1, where TROPOMI shows a narrower range of NO_2 values across all distances. This difference could stem from the fact that the interquartile ranges in Fig. 1 measure the spread of absolute values, while the coefficient of variation accounts for variability relative to the mean. Together, these metrics reveal that TROPOMI may not fully capture localized extremes (narrower IQR) but still captures more relative variability in pollution near interstates than monitors (higher CV).

	Road Type	Monitor CV	TROPOMI CV	JSD	# of Monitors
a) 50-m Buffer	Interstate	75.07	92.60	0.158	58
	Highway	96.27	91.61	0.095	17
	Non-roadway	118.17	106.16	0.009	428
b) 300-m Buffer	Interstate	77.20	91.014	0.133	91
	Highway	135.76	92.31	0.017	90
	Non-roadway	116.23	108.43	0.008	320

Table 1. Coefficient of variation (%) and Jensen-Shannon divergence for all seasons combined at interstate, highway, and non-roadway monitors 2019-2023 for the 50-m and 300-m roadway buffers.

The key differences seen within the JSD across the three monitor classifications are also present in the percent frequency distributions of NO_2 measured by ground-based monitors and TROPOMI (Figure S5), with interstate monitors having the lowest alignment (JSD = 0.158), highway monitors having better alignment (JSD = 0.095), and non-roadway monitors having the best alignment (JSD = 0.009). The strong alignment between TROPOMI and monitor distributions in non-roadway regions is consistent with previous studies (Dressel et al., 2022;

Kim et al., 2024; Ialongo et al., 2020). This close alignment may be due to the relatively lower NO_2 concentrations, which TROPOMI captures more accurately compared to regions with higher emissions. These findings further align with previous work showing that TROPOMI tends to underestimate NO_2 in high-pollution areas (such as interstates and highways) but slightly overestimates in areas of lower pollution, such as rural areas (Dressel et al., 2022; Ialongo et al., 2020; Goldberg et al., 2024).

Due to the large jump in NO_2 levels seen within Fig. 1 in the 50-300m category, we compare the 50-meter buffer roadway classifications (Figure S5; Table 1a) with the 300-meter buffer classifications (Figure S6; Table 1b). Notable differences emerge between distributions, particularly in the highway category, where 73 monitors are added to the highway distribution (increasing from 17 to 90 monitors; Table 1) due to the larger buffer. The alignment between monitor data and TROPOMI observations is significantly improved within the 300-meter buffer near highways. This improvement in alignment is likely due to the decay of NO_2 with increasing distance from the road (Karner et al., 2010; Kimbrough et al., 2017; Richmond-Bryant et al., 2017). Consequently, the lower surface NO_2 concentrations observed at 300 meters are better captured by TROPOMI. This is reflected in Table 1, which shows a substantial reduction in the JSD for highway monitors, from 0.095 in the 50-meter buffer to 0.017 in the 300-meter buffer (an 82% increase in alignment at the 300-meter buffer).

The differences observed in the highway category with the 300-meter buffer may be present since the distribution includes 73 more monitors than the 50-meter buffer, capturing lower NO_2 amounts that are more aligned with TROPOMI's observations. On the other hand, the interstates category exhibits less noticeable change, with only 33 additional monitors in the 300-meter buffer distribution (increasing from 58 in the 50-meter buffer, Table 1a; to 91 in the 300-meter buffer, Table 1b). This suggests that the monitors added in the 300-meter buffer for interstates measure NO_2 levels similar to those already captured in the 50-meter buffer, resulting in little change to the overall distribution.

These results indicate that TROPOMI follows the trend of NO_2 decreasing with increasing distance from roadways that ground-based monitors record, and TROPOMI captures surface concentrations best in winter and at 300+ meters away from the traffic source.

3.2 Column-Column Daily Alignment

Here we compare the distributions of NO_2 from TROPOMI and TEMPO with ground-based monitors to assess how well each satellite instrument captures daily variations in NO_2 concentrations. Our results indicate that TEMPO consistently aligns more closely with ground-based measurements than TROPOMI, particularly in high NO_2 areas such as highways and interstates.

Figure 3 shows the distributions of NO_2 as measured by AQS ground-based monitors (filtered to match valid TROPOMI and TEMPO data), TROPOMI, and TEMPO, separated by road classifications (interstates, highways, and non-roadways) for December 2023 and July 2024. The 1 pm and 2 pm UTC (based on time zone) TEMPO and AQS values were averaged to align with the TROPOMI overpass time of ~1:30 pm LT (see Sect. 2.3). The monitor data in each comparison differs due to the data filtering (see Sect. 2.2 and 2.3). The comparison of frequency distributions reveals how well TEMPO and TROPOMI capture the wide range of ground-based monitor readings across these classifications and time periods.

In December 2023, TEMPO (JSD = 0.007) and TROPOMI (JSD = 0.021) exhibit distinct differences in how well they capture NO_2 distributions across the various road classifications. Near interstates, TEMPO has a 90^{th} percentile at 18.34 x 10^{15} molecules/cm^2 whereas the TROPOMI 90^{th} percentile is 11.27 x 10^{15} molecules/cm^2. TEMPO aligns more closely with monitor distributions with a JSD of 0.066 compared to the TROPOMI JSD of 0.145 (Figure 3). TEMPO has 21.42% of data points above 11 x 10^{15} molecules/cm^2 for interstate values in December, whereas TROPOMI appears to underestimate the frequency of higher NO_2 levels more, with a cumulative frequency of 10.53% above that threshold. Near highways, the TEMPO 90^{th} percentile is 14.70 x 10^{15} molecules/cm^2 compared to TROPOMI with a 90^{th} percentile of 10.06 x 10^{15} molecules/cm^2. The JSD for TEMPO is 0.049 and TROPOMI is 0.125 for highway monitors, indicating that TEMPO has much better alignment on highways (Figure 3). For non-roadway locations, both instruments show very good alignment (TEMPO JSD = 0.005; TROPOMI JSD = 0.012; Figure 3) with the monitor data distributions, but with TEMPO again being slightly better.

In July 2024, the patterns show greater divergence across road classifications (TEMPO JSD = 0.027; TROPOMI JSD = 0.049) between the satellite observations and ground-based monitor data compared to the December 2023 distributions. Near interstates, the TEMPO 90th percentile is 8.46 x 10^{15} molecules/cm^2 and the TROPOMI 90th percentile is 5.58 x 10^{15} molecules/cm^2, with TEMPO aligning more closely (JSD of 0.133 compared to TROPOMI JSD of 0.265; Figure 3). TEMPO has 17.01% of data points above 7 x 10^{15} molecules/cm^2 for interstate values in July, whereas TROPOMI appears to underestimate the frequency of higher NO_2 levels more, with a cumulative frequency of 3.61% above that threshold. Near highways, TEMPO achieves a much better representation of the higher observed NO_2 with a 90th percentile of 9.34 x 10^{15} molecules/cm^2 compared to TROPOMI with a 90th percentile of 5.32 x 10^{15} molecules/cm^2. The JSD for TEMPO is 0.151 and TROPOMI is 0.201 for highway monitors, indicating that TEMPO has better alignment near highways. For non-roadway locations, both instruments show very good alignment (TEMPO JSD = 0.024; TROPOMI JSD = 0.023; Figure 3) with the monitor data distributions, with TEMPO and TROPOMI alignment with ground monitors being more comparable than in December 2023.

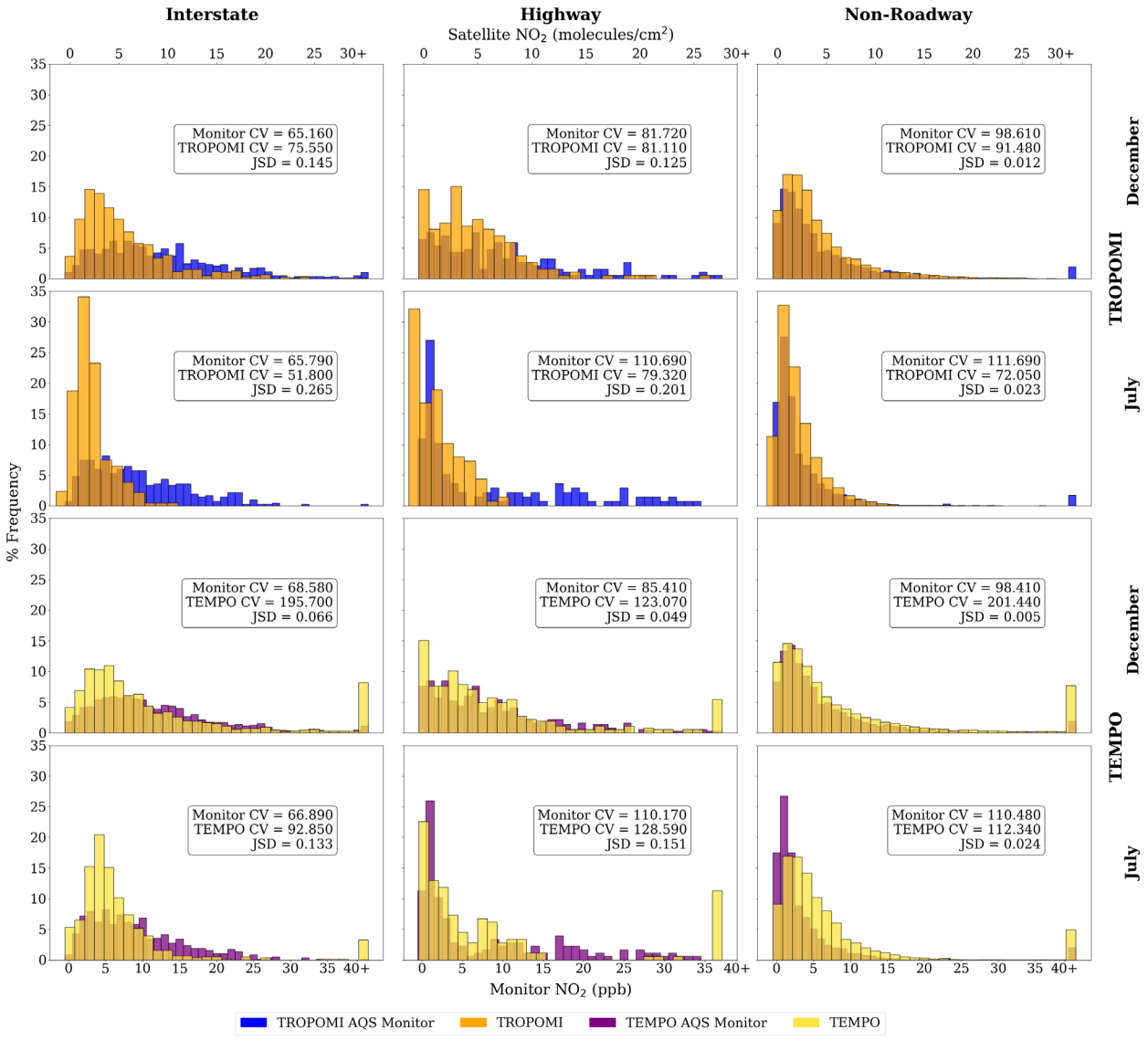

Figure 3. December 2023 and July 2024 at the TROPOMI overpass time (~13:30 LST) frequency distributions of NO_2 as measured by AQS ground-based monitors filtered to the valid TROPOMI (blue) and TEMPO (purple), TROPOMI (light orange), and TEMPO (yellow) data for three monitor classifications: Interstate, Highway, and Non-roadway. The x-axes indicate the range of NO_2, with the primary, lower x-axis showing monitor NO_2 concentrations in parts per billion (ppb) and the secondary, upper x-axis showing TROPOMI NO_2 VCD and TEMPO NO_2 VCD in 10^{15} molecules per cm^2. The boxes show the Coefficient of Variation (CV) and Jensen Shannon Divergence (JSD) for each season and monitor classification.

Throughout both December 2023 and July 2024, TEMPO's improved alignment with ground-based monitors compared to TROPOMI may be attributed to several factors. TEMPO operates from a geostationary orbit, allowing it to take hourly measurements and capture the diurnal variability of NO_2 concentrations more effectively than TROPOMI, which has a single daily overpass time. This high temporal resolution enables TEMPO to better match the timing of NO_2 peaks and fluctuations detected by ground-based monitors, which are also recorded on an hourly basis. Additionally, TEMPO's finer spatial resolution, approximately 2 km in the north-south direction and 4.5 km in the east-west direction, may allow it to capture more localized pollution sources, such as traffic emissions along highways and interstates. This may be why we see such a large difference in alignment in the interstate and highway categories between TEMPO and TROPOMI, and very little difference in alignment in the non-road category. In contrast, TROPOMI's 4 km x 4 km (re-gridded) resolution and single overpass time may be less effective at capturing these localized variations. TEMPO's finer resolution in one direction and its frequent observations may enable it to more precisely match the spatial and temporal variability detected by ground-based monitors. The consistency of slight underestimation for both instruments in high-pollution areas like highways and interstates suggests challenges in fully capturing elevated NO_2 levels that occur near traffic sources. Overall, this indicates that while TEMPO generally provides a closer approximation of NO_2 distributions compared to TROPOMI, both satellite instruments show limitations, particularly in representing peak concentrations at high-polluting sites.

3.3 Column-Surface Diurnal Alignment

In this section we explore the hourly alignment between monitor and hourly TEMPO distributions at interstate, highway, and non-roadway monitors. We find that TEMPO aligns best with ground monitors around midday and exhibits poorer alignment in the early morning and early evening.

Figure 4 presents the hourly JSD for TEMPO NO_2 measurements compared with ground monitors categorized by interstate (red), highway (orange), and non-roadway (green) monitors for December 2023 (Figure 4a) and July 2024 (Figure 4b). The results highlight distinct diurnal

patterns across road types and seasons, reflecting the influence of traffic emissions, atmospheric mixing, and insolation.

In December 2023, all monitor categories exhibit similar trends in the early morning, with high JSD values (highway JSD = 0.358; interstate JSD = 0.331; non-road JSD = 0.210) indicative of moderate to poor alignment between TEMPO and ground-based monitors. This pattern, consistent with early morning rush hour emissions and limited atmospheric vertical mixing (Harkey and Holloway, 2024) as well as a decrease in TEMPO's measurement accuracy due to high solar zenith angles in the morning according to TEMPO documentation (NASA Langley Research Center, 2024), suggests that TEMPO may not capture rapid increases in NO_2 during high traffic and low mixing periods. By mid-morning, JSD has decreased for all road types (highway JSD = 0.085; interstate JSD = 0.067; non-road JSD = 0.027), indicative of good alignment, with non-road monitors showing the most significant improvement (87% increase in alignment). This pattern of better alignment in non-road monitor areas could be attributed to lower NO_2 levels away from major sources of emissions. As the day progresses in December, JSD values for highway and interstate monitors increase steadily (with highways fluctuating more) after 17 UTC (~12 pm LT), with highways increasing in JSD from 0.102 to 0.490 and interstates increasing from JSD 0.097 to 0.590, indicating worsening alignment in the afternoon and early evening. This pattern may reflect the re-accumulation of NO_2 due to afternoon traffic and the collapse of the boundary layer later in the afternoon (Harkey and Holloway, 2024), as well as the decrease in TEMPO's measurement accuracy in the evening (NASA Langley Research Center, 2024). Non-road monitors show less change in JSD throug the day, suggesting that TEMPO alignment is more consistent in non-road monitor areas throughout the rest of the day, only fluctuating in JSD values between 0.009 and 0.05.

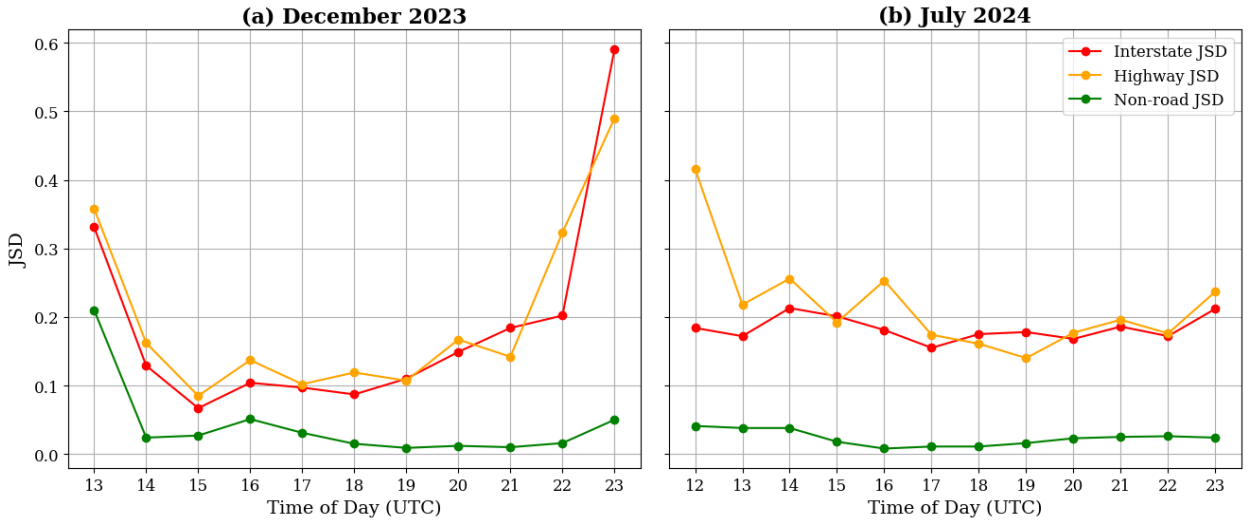

Figure 4. The a) December 2023 and b) July 2024 hourly (UTC) TEMPO NO_2 Jensen-Shannon Divergences at interstate (red), highway (orange), and non-roadway (green) monitor locations.

In July 2024 highway and interstate monitors do not exhibit a clear diurnal pattern, with JSD values fluctuating between 0.14 and 0.416 for highways and 0.155 and 0.212 for interstates throughout the day. Consistent, localized traffic emissions and the shorter NO_2 lifetime during the summer suggest a less variable distribution of NO_2. Non-road monitors in July show somewhat worse alignment in the morning (JSD = 0.041), with improved agreement during the late morning and early afternoon (JSD ranging between 0.008 and 0.025). The non-road JSD remains fairly constant into the early evening, with alignment decreasing by about 13%, indicating that sunlight may play a larger role in the alignment in the evening since the sun is at a higher position in the sky during this time in the summer than in the winter (which increases in JSD at this time), enhancing TEMPO's measurement accuracy in the early evening in July.

Both months exhibit their highest JSDs, and worst alignment, in the early morning or early evening hours, which coincides with peak traffic times and the most uncertainty in TEMPO observations caused by the solar zenith angle. The best alignment and lowest JSDs occur sometime near midday (~10 am LT to ~2 pm LT).

The disparity between highways and interstates in TEMPO, where highways generally have the highest JSD, differs from the pattern seen with TROPOMI, where interstates tended to consistently exhibit worse alignment. This suggests that TEMPO's higher spatial and temporal

resolution may capture localized sources more effectively, leading to variations in alignment based on the distribution and intensity of NO_2 sources.

4 Conclusions

This study evaluates the distributional alignment among estimates of NO_2 abundance from TROPOMI, TEMPO, and ground monitors to inform the potential of satellite data for both regulatory and public health applications, particularly in informing future NO_2 monitor siting strategies. Several limitations and sources of uncertainty should be considered. Several limitations of this analysis include: (1) The overrepresentation of AQS monitors in urban areas; (2) the temporal mismatch between satellite and ground measurements; and (3) the distance from roads analysis doesn't consider other local factors. A key limitation is the overrepresentation of urban areas in the AQS monitoring network, which may bias our results toward urban areas. Since AQS monitors are more densely located in urban regions with high emissions and complex local sources, the results may not fully capture alignment in more rural areas with fewer monitoring stations. Another important consideration is the slight temporal mismatch between satellite and ground-based measurements. TROPOMI provides a single daily observation around 13:30 pm local solar time, whereas ground monitors and TEMPO record NO_2 concentrations throughout the day. To better align with TROPOMI's overpass, we averaged 1 pm and 2 pm LT TEMPO and ground monitor NO_2 values. Since NO_2 concentrations can change rapidly due to meteorological conditions and emissions variability, this averaging approach may introduce some error in comparisons between TEMPO, TROPOMI, and ground-based measurements. The classification of monitors by distance from roads is based on buffer analysis, which does not account for local factors such as wind direction, terrain, proximity to industry, and traffic density, all of which influence NO_2 dispersion. Despite these uncertainties, our findings highlight patterns in column-surface NO_2 agreement and demonstrate the potential for satellite data to complement ground-based monitoring.

The Jensen-Shannon Divergence (JSD) offers a robust and interpretable metric for comparing the alignment and similarity of NO_2 distributions. Its symmetry and bounded range allowed us to evaluate the degree of similarity between satellite and monitor NO_2 values across different spatial and temporal scales, providing a clear quantitative framework for assessing the similarity of two different instruments.

Past studies comparing surface and satellite NO_2 have found temporal correlation of daily values at individual sites ranging from r=0.61 to r=0.69 (Lamsal et al., 2014; Lamsal et al., 2015), monthly and seasonal values at individual sites ranging from r=0.67 to r=0.90 (Griffin et al., 2019; Yu & Li, 2022; Harkey & Holloway, 2024; Dressel et al., 2022; Xu & Xiang, 2023; Lamsal et al., 2015), and annual average values at sites ranging from r=0.68 to r=0.93 (Zhang et al., 2018; Lamsal et al., 2015; Goldberg et al., 2021; Kim et al., 2024; Bechle et al., 2013; H. J. Lee et al., 2023). Here, r refers to the Pearson correlation coefficient, which measures the strength and direction of a linear relationship between variables. In some cases, these comparisons adjusted column values to the surface (e.g. Lamsal et al., 2014) and/or adjusted ground-monitors to reduce the error in chemiluminescent detection of NO_2 (e.g. Lamsal et al., 2015; Bechle et al., 2013). Using similar methods, TROPOMI tends to show better agreement with annual AQS NO_2 than does OMI, e.g. r=0.81 using TROPOMI (Goldberg et al., 2015) versus r=0.68 from OMI (Lamsal et al., 2015). Off-road AQS monitors tend to show better agreement with satellite data than near-road AQS monitors, e.g. r = 0.81-0.87 at non-near-road sites versus r = 0.64-0.74 at near-road sites (Kim et al., 2024). The underestimation of estimated near-surface NO_2 near roads and localized sources is a recurring issue in OMI and TROPOMI NO_2 VCDs (Dressel et al., 2022; Goldberg et al., 2024; Ialongo et al., 2020).

In this study, we find a pattern of decreasing NO_2 with increasing distance from traffic sources, which is consistent with the findings of previous studies (Kimbrough et al., 2017; Karner et al., 2010; Richmond-Bryant et al., 2017). While ground-based monitors and TROPOMI satellite data may differ with proximity to roadways, particularly within 50-m, their measurements still follow the same overall trend. This convergence with increasing distance may be due to the reduction of localized near-road emissions and the broader atmospheric mixing captured more effectively by satellite observations at greater distances from roads. Using a larger buffer distance from roads (300 meters instead of 50 meters) improves the alignment between TROPOMI and monitor data, especially for highway monitor locations (JSD decreases by ~82%). The overall trend reflects the well-established gradient of declining NO_2 levels with increasing distance from traffic sources, and TROPOMI's ability to capture this trend, even if the specific values differ from AQS monitors in the near-road environment. Our findings indicate that TROPOMI tends to slightly underestimate surface NO_2 concentrations in areas with high traffic, such as interstates and highways, due to its spatial resolution and full-column measurements, which smooth out

localized, ground-level pollution peaks captured by ground monitors. This is most evident in interstate monitors, where the JSD reveals the greatest divergence between satellite and monitor data (JSD = 0.158). These results are consistent with prior studies (Dressel et al., 2022; Kim et al., 2024; Ialongo et al., 2020), which also found that satellite instruments are less effective at capturing high NO_2 events near localized sources like traffic. The distributional alignment improves in non-roadway monitors (JSD = 0.009), where NO_2 levels are lower, and there are usually fewer localized sources of pollution. The lower pollution levels in these areas allow TROPOMI to more accurately reflect the conditions captured by ground-based monitors, leading to lower JSD values, and therefore better alignment. This trend suggests that TROPOMI may be particularly useful for monitoring air quality in rural or less polluted regions where ground monitors are sparse or absent.

Seasonality plays a critical role in the similarity of satellite and monitor data. Winter consistently shows the best alignment (JSD = 0.010), with the TROPOMI distribution capturing nearly the full gradient of NO_2 seen within the ground-based monitor distribution. This likely reflects the longer atmospheric lifetime of NO_2 in winter, which allows for better vertical mixing and less spatial variability (Harkey et al., 2015; Boersma et al., 2009; Shah et al., 2020). In contrast, summer shows the worst alignment (JSD = 0.035), which is likely due to the shorter lifetime of NO_2 and increased photochemical activity during warmer months, causing greater discrepancies between localized surface measurements and the satellite column. Similar conclusions were reached by previous studies (Shah et al., 2020; Karagkiozidis et al., 2023), indicating that seasonality is a crucial factor in assessing satellite performance for regulatory purposes. These seasonal differences underscore the need for considering temporal factors when evaluating the use of satellite data for monitor siting and NO_2 regulation.

The integration of TEMPO data into this study highlights its potential to advance our understanding of NO_2 distributions, especially when compared to TROPOMI. TEMPO's ability to provide hourly measurements at a finer spatial resolution offers significant advantages in capturing diurnal NO_2 patterns and detecting localized pollution events. Our findings from December 2023 and July 2024 at the TROPOMI overpass time (~13:30 LST) demonstrate that TEMPO better captures the wide range of surface NO_2 measurements than TROPOMI, especially at higher NO_2 levels. TEMPO's JSDs are almost always lower than TROPOMI's, with

JSDs ranging from 0.005 to 0.151 and TROPOMI's JSDs ranging from 0.012 to 0.265. This improvement in alignment with ground monitors could be attributed to TEMPO's better spatial and temporal resolution.

We also find that TEMPO is best at capturing ground-level NO_2 amounts around midday (~10 am to ~2 pm LT). This could be due to the lower traffic levels and therefore lower pollution levels during this time period, as well as a lower solar zenith angle, allowing TEMPO to have more accurate measurements. However, challenges remain in completely capturing high NO_2 levels during peak traffic times and accurately capturing NO_2 during high solar zenith angles in the morning and evening across monitor classifications. These results underscore the influence of spatial resolution, time of day, and measurement frequency on the ability of satellite instruments to align with ground-based NO_2 measurements. Future research should build upon these insights by incorporating longer time periods and multiple years of data as more TEMPO data becomes available to study long-term TEMPO distributions. The enhanced temporal and spatial resolution of TEMPO, alongside its comparison to other instruments like TROPOMI, provides valuable context for understanding the dynamics of NO_2 pollution, especially how it varies throughout the day. Spatially contiguous satellite products and our analysis of air quality variability offer the potential to support air quality managers and public health analysis.

Code and Data Availability

All data used in this study are open to the public. Hourly NO_2 data from AQS were obtained from https://aqs.epa.gov/aqsweb/airdata/download_files.html. Copernicus Sentinel 5P Level 2 TROPOMI NO_2 data were processed by the ESA, Koninklijk Nederlands Meteorologisch Instituut (KNMI; https://doi.org/10.5270/S5P-s4ljg54), downloaded from the NASA Goddard Earth Sciences Data and Information Center (GES DISC) in January 2021, and gridded using WHIPS (https://sage.nelson.wisc.edu/data-and-models/wisconsin-horizontal-interpolation-program-for-satellites-whips/). TEMPO Level 3 NO_2 data were downloaded from NASA's EarthData Search (https://search.earthdata.nasa.gov/search/granules?p=C2930763263-LARC_CLOUD&pg[0][v]=f&tl=1732652660.361!3!!). The 2021 Primary and Secondary Roads Tiger/Line state-level shapefiles were downloaded from the U.S. Census Bureau (https://www.census.gov/cgi-bin/geo/shapefiles/index.php?year=2021&layergroup=Roads).

Since all of our data is publicly available and the methods describe our calculations in detail, we did not make our code publicly available. The Jensen Shannon Divergence was calculated using the *scipy.spatial.distance.jensenshannon* python package.

Author Contribution

SA and TH conceptualized and designed methodology. MH helped with data curation. SA performed data analysis and visualization and prepared the original draft of the manuscript. All authors contributed to reviewing and editing the manuscript.

Competing Interests

The authors declare that they have no conflict of interest.

Acknowledgements

This paper was funded by NASA Grant 80NSSC21K0427 through the Health and Air Quality Applied Sciences Team (HAQAST). We also thank the EPA for providing the Air Quality System data, the Earth Sciences Data and Information Center (GES DISC) for TROPOMI L2 data, the Wisconsin Horizontal Interpolation Program for Satellites (WHIPS) for helping to process and grid TROPOMI data, and NASA Langley Atmospheric Science Data Center Distributed Active Archive Center for providing access to the TEMPO data. The authors acknowledge OpenAI 4o for help with data analysis debugging. We also appreciate valuable comments from Muhammad Omar Nawaz and anonymous reviewers from the public discussion.

References

Achakulwisut, P., Brauer, M., Hystad, P., and Anenberg, S. C.: Global, national, and urban burdens of paediatric asthma incidence attributable to ambient NO2 pollution: estimates from global datasets, The Lancet Planetary Health, 3, e166–e178, https://doi.org/10.1016/S2542-5196(19)30046-4, 2019.

Aerts, S., Haesbroeck, G., and Ruwet, C.: Multivariate coefficients of variation: Comparison and influence functions, Journal of Multivariate Analysis, 142, 183–198, https://doi.org/10.1016/j.jmva.2015.08.006, 2015.

Ahmed, Z., Zeeshan, S., Persaud, N., Degroat, W., Abdelhalim, H., and Liang, B. T.: Investigating genes associated with cardiovascular disease among heart failure patients for translational research and precision medicine, Clinical and Translational Dis, 3, e206, https://doi.org/10.1002/ctd2.206, 2023.

Anenberg, S. C., Mohegh, A., Goldberg, D. L., Kerr, G. H., Brauer, M., Burkart, K., Hystad, P., Larkin, A., Wozniak, S., and Lamsal, L.: Long-term trends in urban NO2 concentrations and associated paediatric asthma incidence: estimates from global datasets, The Lancet Planetary Health, 6, e49–e58, https://doi.org/10.1016/S2542-5196(21)00255-2, 2022.

Bai, L., Chen, H., Hatzopoulou, M., Jerrett, M., Kwong, J. C., Burnett, R. T., Van Donkelaar, A., Copes, R., Martin, R. V., Van Ryswyk, K., Lu, H., Kopp, A., and Weichenthal, S.: Exposure to Ambient Ultrafine Particles and Nitrogen Dioxide and Incident Hypertension and Diabetes:, Epidemiology, 29, 323–332, https://doi.org/10.1097/EDE.0000000000000798, 2018.

Bechle, M. J., Millet, D. B., and Marshall, J. D.: Remote sensing of exposure to NO2: Satellite versus ground-based measurement in a large urban area, Atmospheric Environment, 69, 345–353, https://doi.org/10.1016/j.atmosenv.2012.11.046, 2013.

Behera, S. N. and Sharma, M.: Transformation of atmospheric ammonia and acid gases into components of PM2.5: an environmental chamber study, Environ Sci Pollut Res, 19, 1187–1197, https://doi.org/10.1007/s11356-011-0635-9, 2012.

Boersma, K. F., Jacob, D. J., Trainic, M., Rudich, Y., DeSmedt, I., Dirksen, R., and Eskes, H. J.: Validation of urban NO₂ concentrations and their diurnal and seasonal variations observed from the SCIAMACHY and OMI sensors using in situ surface measurements in Israeli cities, Atmos. Chem. Phys., 9, 3867–3879, https://doi.org/10.5194/acp-9-3867-2009, 2009.

Boersma, K. F., Eskes, H. J., Richter, A., De Smedt, I., Lorente, A., Beirle, S., Van Geffen, J. H. G. M., Zara, M., Peters, E., Van Roozendael, M., Wagner, T., Maasakkers, J. D., Van Der A, R. J.,

Nightingale, J., De Rudder, A., Irie, H., Pinardi, G., Lambert, J.-C., and Compernolle, S. C.: Improving algorithms and uncertainty estimates for satellite NO₂ retrievals: results from the quality assurance for the essential climate variables (QA4ECV) project, Atmos. Meas. Tech., 11, 6651–6678, https://doi.org/10.5194/amt-11-6651-2018, 2018.

Camilleri, S. F., Kerr, G. H., Anenberg, S. C., and Horton, D. E.: All-Cause NO_2 -Attributable Mortality Burden and Associated Racial and Ethnic Disparities in the United States, Environ. Sci. Technol. Lett., 10, 1159–1164, https://doi.org/10.1021/acs.estlett.3c00500, 2023.

Wisconsin Horizontal Interpolation Program for Satellites (WHIPS): https://sage.nelson.wisc.edu/data-and-models/wisconsin-horizontal-interpolation-program-for-satellites-whips/, last access: 6 December 2024.

Chance, K., Liu, X., Miller, C. C., González Abad, G., Huang, G., Nowlan, C., Souri, A., Suleiman, R., Sun, K., Wang, H., Zhu, L., Zoogman, P., Al-Saadi, J., Antuña-Marrero, J.-C., Carr, J., Chatfield, R., Chin, M., Cohen, R., Edwards, D., Fishman, J., Flittner, D., Geddes, J., Grutter, M., Herman, J. R., Jacob, D. J., Janz, S., Joiner, J., Kim, J., Krotkov, N. A., Lefer, B., Martin, R. V., Mayol-Bracero, O. L., Naeger, A., Newchurch, M., Pfister, G. G., Pickering, K., Pierce, R. B., Rivera Cárdenas, C., Saiz-Lopez, A., Simpson, W., Spinei, E., Spurr, R. J. D., Szykman, J. J., Torres, O., and Wang, J.: TEMPO Green Paper: Chemistry, physics, and meteorology experiments with the Tropospheric Emissions: monitoring of pollution instrument, in: Sensors, Systems, and Next-Generation Satellites XXIII, Sensors, Systems, and Next-Generation Satellites XXIII, Strasbourg, France, 10, https://doi.org/10.1117/12.2534883, 2019.

Chowdhury, S., Haines, A., Klingmüller, K., Kumar, V., Pozzer, A., Venkataraman, C., Witt, C., and Lelieveld, J.: Global and national assessment of the incidence of asthma in children and adolescents from major sources of ambient NO_2, Environ. Res. Lett., 16, 035020, https://doi.org/10.1088/1748-9326/abe909, 2021.

Clim, A., Zota, R. D., and TinicĂ, G.: The Kullback-Leibler Divergence Used in Machine Learning Algorithms for Health Care Applications and Hypertension Prediction: A Literature Review, Procedia Computer Science, 141, 448–453, https://doi.org/10.1016/j.procs.2018.10.144, 2018.

784 Cooper, M. J., Martin, R. V., McLinden, C. A., and Brook, J. R.: Inferring ground-level nitrogen
785 dioxide concentrations at fine spatial resolution applied to the TROPOMI satellite instrument,
786 Environ. Res. Lett., 15, 104013, https://doi.org/10.1088/1748-9326/aba3a5, 2020.

787 Dang, R., Jacob, D. J., Shah, V., Eastham, S. D., Fritz, T. M., Mickley, L. J., Liu, T., Wang, Y.,
788 and Wang, J.: Background nitrogen dioxide (NO_2) over the United States and its implications for
789 satellite observations and trends: effects of nitrate photolysis, aircraft, and open fires, Atmos.
790 Chem. Phys., 23, 6271–6284, https://doi.org/10.5194/acp-23-6271-2023, 2023.

791 Dressel, I. M., Demetillo, M. A. G., Judd, L. M., Janz, S. J., Fields, K. P., Sun, K., Fiore, A. M.,
792 McDonald, B. C., and Pusede, S. E.: Daily Satellite Observations of Nitrogen Dioxide Air
793 Pollution Inequality in New York City, New York and Newark, New Jersey: Evaluation and
794 Application, Environ. Sci. Technol., 56, 15298–15311, https://doi.org/10.1021/acs.est.2c02828,
795 2022.

796 Duncan, B. N., Yoshida, Y., De Foy, B., Lamsal, L. N., Streets, D. G., Lu, Z., Pickering, K. E.,
797 and Krotkov, N. A.: The observed response of Ozone Monitoring Instrument (OMI) NO2
798 columns to NOx emission controls on power plants in the United States: 2005–2011,
799 Atmospheric Environment, 81, 102–111, https://doi.org/10.1016/j.atmosenv.2013.08.068, 2013.

800 Duncan, B. N., Prados, A. I., Lamsal, L. N., Liu, Y., Streets, D. G., Gupta, P., Hilsenrath, E.,
801 Kahn, R. A., Nielsen, J. E., Beyersdorf, A. J., Burton, S. P., Fiore, A. M., Fishman, J., Henze, D.
802 K., Hostetler, C. A., Krotkov, N. A., Lee, P., Lin, M., Pawson, S., Pfister, G., Pickering, K. E.,
803 Pierce, R. B., Yoshida, Y., and Ziemba, L. D.: Satellite data of atmospheric pollution for U.S. air
804 quality applications: Examples of applications, summary of data end-user resources, answers to
805 FAQs, and common mistakes to avoid, Atmospheric Environment, 94, 647–662,
806 https://doi.org/10.1016/j.atmosenv.2014.05.061, 2014.

807 Dunlea, E. J., Herndon, S. C., Nelson, D. D., Volkamer, R. M., San Martini, F., Sheehy, P. M.,
808 Zahniser, M. S., Shorter, J. H., Wormhoudt, J. C., Lamb, B. K., Allwine, E. J., Gaffney, J. S.,
809 Marley, N. A., Grutter, M., Marquez, C., Blanco, S., Cardenas, B., Retama, A., Ramos Villegas,
810 C. R., Kolb, C. E., Molina, L. T., and Molina, M. J.: Evaluation of nitrogen dioxide
811 chemiluminescence monitors in a polluted urban environment, Atmos. Chem. Phys., 7, 2691–
812 2704, https://doi.org/10.5194/acp-7-2691-2007, 2007.

AirData Pre-Generated Hourly File Downloads: https://aqs.epa.gov/aqsweb/airdata/download_files.html#Raw, last access: 21 February 2025.

European Space Agency: TROPOMI Level 2 Nitrogen Dioxide, https://doi.org/10.5270/S5P-9bnp8q8, 2021.

Fontijn, Arthur., Sabadell, A. J., and Ronco, R. J.: Homogeneous chemiluminescent measurement of nitric oxide with ozone. Implications for continuous selective monitoring of gaseous air pollutants, Anal. Chem., 42, 575–579, https://doi.org/10.1021/ac60288a034, 1970.

Frost, G. J., McKeen, S. A., Trainer, M., Ryerson, T. B., Neuman, J. A., Roberts, J. M., Swanson, A., Holloway, J. S., Sueper, D. T., Fortin, T., Parrish, D. D., Fehsenfeld, F. C., Flocke, F., Peckham, S. E., Grell, G. A., Kowal, D., Cartwright, J., Auerbach, N., and Habermann, T.: Effects of changing power plant NO_x emissions on ozone in the eastern United States: Proof of concept, J. Geophys. Res., 111, 2005JD006354, https://doi.org/10.1029/2005JD006354, 2006.

Gantt, B., Owen, R. C., and Watkins, N.: Characterizing Nitrogen Oxides and Fine Particulate Matter near Major Highways in the United States Using the National Near-Road Monitoring Network, Environ. Sci. Technol., 55, 2831–2838, https://doi.org/10.1021/acs.est.0c05851, 2021.

Ge, B., Sun, Y., Liu, Y., Dong, H., Ji, D., Jiang, Q., Li, J., and Wang, Z.: Nitrogen dioxide measurement by cavity attenuated phase shift spectroscopy (CAPS) and implications in ozone production efficiency and nitrate formation in Beijing, China, JGR Atmospheres, 118, 9499–9509, https://doi.org/10.1002/jgrd.50757, 2013.

Goldberg, D. L., Anenberg, S. C., Kerr, G. H., Mohegh, A., Lu, Z., and Streets, D. G.: TROPOMI NO_2 in the United States: A Detailed Look at the Annual Averages, Weekly Cycles, Effects of Temperature, and Correlation With Surface NO_2 Concentrations, Earth's Future, 9, e2020EF001665, https://doi.org/10.1029/2020EF001665, 2021.

Goldberg, D. L., Tao, M., Kerr, G. H., Ma, S., Tong, D. Q., Fiore, A. M., Dickens, A. F., Adelman, Z. E., and Anenberg, S. C.: Evaluating the spatial patterns of U.S. urban NOx emissions using TROPOMI NO2, Remote Sensing of Environment, 300, 113917, https://doi.org/10.1016/j.rse.2023.113917, 2024.

Griffin, D., Zhao, X., McLinden, C. A., Boersma, F., Bourassa, A., Dammers, E., Degenstein, D., Eskes, H., Fehr, L., Fioletov, V., Hayden, K., Kharol, S. K., Li, S., Makar, P., Martin, R. V., Mihele, C., Mittermeier, R. L., Krotkov, N., Sneep, M., Lamsal, L. N., Linden, M. T., Geffen, J. V., Veefkind, P., and Wolde, M.: High-Resolution Mapping of Nitrogen Dioxide With TROPOMI: First Results and Validation Over the Canadian Oil Sands, Geophysical Research Letters, 46, 1049–1060, https://doi.org/10.1029/2018GL081095, 2019.

Grulke, N. E. and Heath, R. L.: Ozone effects on plants in natural ecosystems, Plant Biol J, 22, 12–37, https://doi.org/10.1111/plb.12971, 2020.

Hales, S., Atkinson, J., Metcalfe, J., Kuschel, G., and Woodward, A.: Long term exposure to air pollution, mortality and morbidity in New Zealand: Cohort study, Science of The Total Environment, 801, 149660, https://doi.org/10.1016/j.scitotenv.2021.149660, 2021.

Harkey, M. and Holloway, T.: Simulated Surface-Column NO_2 Connections for Satellite Applications, JGR Atmospheres, 129, e2024JD041912, https://doi.org/10.1029/2024JD041912, 2024.

Harkey, M., Holloway, T., Oberman, J., and Scotty, E.: An evaluation of CMAQ NO_2 using observed chemistry-meteorology correlations, JGR Atmospheres, 120, https://doi.org/10.1002/2015JD023316, 2015.

Harkey, M., Holloway, T., Kim, E. J., Baker, K. R., and Henderson, B.: Satellite Formaldehyde to Support Model Evaluation, JGR Atmospheres, 126, e2020JD032881, https://doi.org/10.1029/2020JD032881, 2021.

Holloway, T., Miller, D., Anenberg, S., Diao, M., Duncan, B., Fiore, A. M., Henze, D. K., Hess, J., Kinney, P. L., Liu, Y., Neu, J. L., O'Neill, S. M., Odman, M. T., Pierce, R. B., Russell, A. G., Tong, D., West, J. J., and Zondlo, M. A.: Satellite Monitoring for Air Quality and Health, Annu. Rev. Biomed. Data Sci., 4, 417–447, https://doi.org/10.1146/annurev-biodatasci-110920-093120, 2021.

Huangfu, P. and Atkinson, R.: Long-term exposure to NO2 and O3 and all-cause and respiratory mortality: A systematic review and meta-analysis, Environment International, 144, 105998, https://doi.org/10.1016/j.envint.2020.105998, 2020.

Huber, D. E., Steiner, A. L., and Kort, E. A.: Daily Cropland Soil NO_x Emissions Identified by TROPOMI and SMAP, Geophysical Research Letters, 47, e2020GL089949, https://doi.org/10.1029/2020GL089949, 2020.

Ialongo, I., Virta, H., Eskes, H., Hovila, J., and Douros, J.: Comparison of TROPOMI/Sentinel-5 Precursor NO₂ observations with ground-based measurements in Helsinki, Atmos. Meas. Tech., 13, 205–218, https://doi.org/10.5194/amt-13-205-2020, 2020.

Jia, M., Wang, Z., Wang, C., Mao, D., and Zhang, Y.: A New Vegetation Index to Detect Periodically Submerged Mangrove Forest Using Single-Tide Sentinel-2 Imagery, Remote Sensing, 11, 2043, https://doi.org/10.3390/rs11172043, 2019.

Jones, D. C., Danaher, P., Kim, Y., Beechem, J. M., Gottardo, R., and Newell, E. W.: An information theoretic approach to detecting spatially varying genes, Cell Reports Methods, 3, 100507, https://doi.org/10.1016/j.crmeth.2023.100507, 2023.

Kang, D. and Pickering, K.: Lightning NOx Emissions and the Implications for Surface Air Quality over the Contiguous United States, EM (Pittsburgh Pa), 11, 1–6, 2018.

Karagkiozidis, D., Koukouli, M.-E., Bais, A., Balis, D., and Tzoumaka, P.: Assessment of the NO2 Spatio-Temporal Variability over Thessaloniki, Greece, Using MAX-DOAS Measurements and Comparison with S5P/TROPOMI Observations, Applied Sciences, 13, 2641, https://doi.org/10.3390/app13042641, 2023.

Karner, A. A., Eisinger, D. S., and Niemeier, D. A.: Near-Roadway Air Quality: Synthesizing the Findings from Real-World Data, Environ. Sci. Technol., 44, 5334–5344, https://doi.org/10.1021/es100008x, 2010.

Kebabian, P. L., Herndon, S. C., and Freedman, A.: Detection of Nitrogen Dioxide by Cavity Attenuated Phase Shift Spectroscopy, Anal. Chem., 77, 724–728, https://doi.org/10.1021/ac048715y, 2005.

Kerr, G. H., Goldberg, D. L., Harris, M. H., Henderson, B. H., Hystad, P., Roy, A., and Anenberg, S. C.: Ethnoracial Disparities in Nitrogen Dioxide Pollution in the United States: Comparing Data Sets from Satellites, Models, and Monitors, Environ. Sci. Technol., 57, 19532–19544, https://doi.org/10.1021/acs.est.3c03999, 2023.

Kibirige, G. W., Huang, C. C., Liu, C. L., and Chen, M. C.: Influence of land-sea breeze on PM$$_{2.5}$$ prediction in central and southern Taiwan using composite neural network, Sci Rep, 13, 3827, https://doi.org/10.1038/s41598-023-29845-w, 2023.

Kim, E. J., Holloway, T., Kokandakar, A., Harkey, M., Elkins, S., Goldberg, D. L., and Heck, C.: A Comparison of Regression Methods for Inferring Near-Surface NO_2 With Satellite Data, JGR Atmospheres, 129, e2024JD040906, https://doi.org/10.1029/2024JD040906, 2024.

Kim, H. C., Kim, S., Lee, S.-H., Kim, B.-U., and Lee, P.: Fine-Scale Columnar and Surface NOx Concentrations over South Korea: Comparison of Surface Monitors, TROPOMI, CMAQ and CAPSS Inventory, Atmosphere, 11, 101, https://doi.org/10.3390/atmos11010101, 2020.

Kim, M., Brunner, D., and Kuhlmann, G.: Importance of satellite observations for high-resolution mapping of near-surface NO2 by machine learning, Remote Sensing of Environment, 264, 112573, https://doi.org/10.1016/j.rse.2021.112573, 2021.

Kimbrough, S., Chris Owen, R., Snyder, M., and Richmond-Bryant, J.: NO to NO2 conversion rate analysis and implications for dispersion model chemistry methods using Las Vegas, Nevada near-road field measurements, Atmospheric Environment, 165, 23–34, https://doi.org/10.1016/j.atmosenv.2017.06.027, 2017.

Knox, J. B. and Lange, R.: Surface Air Pollutant Concentration Frequency Distributions: Implications for Urban Modeling, Journal of the Air Pollution Control Association, 24, 48–53, https://doi.org/10.1080/00022470.1974.10469893, 1974.

Lamsal, L. N., Krotkov, N. A., Celarier, E. A., Swartz, W. H., Pickering, K. E., Bucsela, E. J., Gleason, J. F., Martin, R. V., Philip, S., Irie, H., Cede, A., Herman, J., Weinheimer, A., Szykman, J. J., and Knepp, T. N.: Evaluation of OMI operational standard NO₂ column retrievals using in situ and surface-based NO₂ observations, Atmos. Chem. Phys., 14, 11587–11609, https://doi.org/10.5194/acp-14-11587-2014, 2014.

Lamsal, L. N., Duncan, B. N., Yoshida, Y., Krotkov, N. A., Pickering, K. E., Streets, D. G., and Lu, Z.: U.S. NO2 trends (2005–2013): EPA Air Quality System (AQS) data versus improved observations from the Ozone Monitoring Instrument (OMI), Atmospheric Environment, 110, 130–143, https://doi.org/10.1016/j.atmosenv.2015.03.055, 2015.

924 Lange, K., Richter, A., and Burrows, J. P.: Variability of nitrogen oxide emission fluxes and
925 lifetimes estimated from Sentinel-5P TROPOMI observations, Atmos. Chem. Phys., 22, 2745–
926 2767, https://doi.org/10.5194/acp-22-2745-2022, 2022.

927 Lee, H. J. and Koutrakis, P.: Daily Ambient NO_2 Concentration Predictions Using Satellite
928 Ozone Monitoring Instrument NO_2 Data and Land Use Regression, Environ. Sci. Technol.,
929 140204134232009, https://doi.org/10.1021/es404845f, 2014.

930 Lee, H. J., Liu, Y., and Chatfield, R. B.: Neighborhood-scale ambient NO2 concentrations using
931 TROPOMI NO2 data: Applications for spatially comprehensive exposure assessment, Science of
932 The Total Environment, 857, 159342, https://doi.org/10.1016/j.scitotenv.2022.159342, 2023.

933 Lee, M., Heikes, B. G., Jacob, D. J., Sachse, G., and Anderson, B.: Hydrogen peroxide, organic
934 hydroperoxide, and formaldehyde as primary pollutants from biomass burning, J. Geophys. Res.,
935 102, 1301–1309, https://doi.org/10.1029/96JD01709, 1997.

936 Levinson, R. and Akbari, H.: Potential benefits of cool roofs on commercial buildings:
937 conserving energy, saving money, and reducing emission of greenhouse gases and air pollutants,
938 Energy Efficiency, 3, 53–109, https://doi.org/10.1007/s12053-008-9038-2, 2010.

939 Li, J., Wang, Y., Zhang, R., Smeltzer, C., Weinheimer, A., Herman, J., Boersma, K. F., Celarier,
940 E. A., Long, R. W., Szykman, J. J., Delgado, R., Thompson, A. M., Knepp, T. N., Lamsal, L. N.,
941 Janz, S. J., Kowalewski, M. G., Liu, X., and Nowlan, C. R.: Comprehensive evaluations of
942 diurnal NO₂ measurements during DISCOVER-AQ 2011: effects of
943 resolution-dependent representation of NO_{<i>x</i>}
944 emissions, Atmos. Chem. Phys., 21, 11133–11160, https://doi.org/10.5194/acp-21-11133-2021,
945 2021.

946 Liu, X., Yi, G., Zhou, X., Zhang, T., Lan, Y., Yu, D., Wen, B., and Hu, J.: Atmospheric NO2
947 Distribution Characteristics and Influencing Factors in Yangtze River Economic Belt: Analysis of
948 the NO2 Product of TROPOMI/Sentinel-5P, Atmosphere, 12, 1142,
949 https://doi.org/10.3390/atmos12091142, 2021.

Melville, P., Yang, S.M., Saar-Tsechansky, M., Mooney, R.J.: Active Learning for Probability Estimation using Jensen-Shannon Divergence, in: Proceedings of the 16th European Conference on Machine Learning, 268–279, 2005.

Menéndez, M. L., Pardo, J. A., Pardo, L., and Pardo, M. C.: The Jensen-Shannon divergence, Journal of the Franklin Institute, 334, 307–318, https://doi.org/10.1016/S0016-0032(96)00063-4, 1997.

Meng, X., Liu, C., Chen, R., Sera, F., Vicedo-Cabrera, A. M., Milojevic, A., Guo, Y., Tong, S., Coelho, M. D. S. Z. S., Saldiva, P. H. N., Lavigne, E., Correa, P. M., Ortega, N. V., Osorio, S., Garcia, Kyselý, J., Urban, A., Orru, H., Maasikmets, M., Jaakkola, J. J. K., Ryti, N., Huber, V., Schneider, A., Katsouyanni, K., Analitis, A., Hashizume, M., Honda, Y., Ng, C. F. S., Nunes, B., Teixeira, J. P., Holobaca, I. H., Fratianni, S., Kim, H., Tobias, A., Íñiguez, C., Forsberg, B., Åström, C., Ragettli, M. S., Guo, Y.-L. L., Pan, S.-C., Li, S., Bell, M. L., Zanobetti, A., Schwartz, J., Wu, T., Gasparrini, A., and Kan, H.: Short term associations of ambient nitrogen dioxide with daily total, cardiovascular, and respiratory mortality: multilocation analysis in 398 cities, BMJ, n534, https://doi.org/10.1136/bmj.n534, 2021.

Mills, I. C., Atkinson, R. W., Kang, S., Walton, H., and Anderson, H. R.: Quantitative systematic review of the associations between short-term exposure to nitrogen dioxide and mortality and hospital admissions, BMJ Open, 5, e006946, https://doi.org/10.1136/bmjopen-2014-006946, 2015.

Mölter, A., Agius, R., De Vocht, F., Lindley, S., Gerrard, W., Custovic, A., and Simpson, A.: Effects of long-term exposure to PM_{10} and NO_2 on asthma and wheeze in a prospective birth cohort, J Epidemiol Community Health, 68, 21–28, https://doi.org/10.1136/jech-2013-202681, 2014.

Mondal, A., Sharma, S. K., Mandal, T. K., Girach, I., and Ojha, N.: Frequency distribution of pollutant concentrations over Indian megacities impacted by the COVID-19 lockdown, Environ Sci Pollut Res, 29, 85676–85687, https://doi.org/10.1007/s11356-021-16874-z, 2022.

Naeger, A. R., Newchurch, M. J., Moore, T., Chance, K., Liu, X., Alexander, S., Murphy, K., and Wang, B.: Revolutionary Air-Pollution Applications from Future Tropospheric Emissions:

Monitoring of Pollution (TEMPO) Observations, Bulletin of the American Meteorological Society, 102, E1735–E1741, https://doi.org/10.1175/BAMS-D-21-0050.1, 2021.

Tropospheric Emissions: Monitoring of Pollution (EVI-1) | NASA's Earth Observing System: https://eospso.nasa.gov/missions/tropospheric-emissions-monitoring-pollution-evi-1, last access: 26 November 2024.

NASA Langley Research Center: TEMPO Level 2/3 trace gas and cloud data user guide, 2024.

Novotny, E. V., Bechle, M. J., Millet, D. B., and Marshall, J. D.: National Satellite-Based Land-Use Regression: NO_2 in the United States, Environ. Sci. Technol., 45, 4407–4414, https://doi.org/10.1021/es103578x, 2011.

Orellano, P., Reynoso, J., Quaranta, N., Bardach, A., and Ciapponi, A.: Short-term exposure to particulate matter (PM10 and PM2.5), nitrogen dioxide (NO2), and ozone (O3) and all-cause and cause-specific mortality: Systematic review and meta-analysis, Environment International, 142, 105876, https://doi.org/10.1016/j.envint.2020.105876, 2020.

Penn, E. and Holloway, T.: Evaluating current satellite capability to observe diurnal change in nitrogen oxides in preparation for geostationary satellite missions, Environ. Res. Lett., 15, 034038, https://doi.org/10.1088/1748-9326/ab6b36, 2020.

Pollack, R.: Studies of Pollutant Concentration Frequency Distributions, 1975.

Qin, M., Yu, H., Hu, Y., Russell, A. G., Odman, M. T., Doty, K., Pour-Biazar, A., McNider, R. T., and Knipping, E.: Improving ozone simulations in the Great Lakes Region: The role of emissions, chemistry, and dry deposition, Atmospheric Environment, 202, 167–179, https://doi.org/10.1016/j.atmosenv.2019.01.025, 2019.

Richmond-Bryant, J., Chris Owen, R., Graham, S., Snyder, M., McDow, S., Oakes, M., and Kimbrough, S.: Estimation of on-road NO2 concentrations, NO2/NOX ratios, and related roadway gradients from near-road monitoring data, Air Qual Atmos Health, 10, 611–625, https://doi.org/10.1007/s11869-016-0455-7, 2017.

Richter, A., Burrows, J. P., Nüß, H., Granier, C., and Niemeier, U.: Increase in tropospheric nitrogen dioxide over China observed from space, Nature, 437, 129–132, https://doi.org/10.1038/nature04092, 2005.

Sangkham, S., Phairuang, W., Sherchan, S. P., Pansakun, N., Munkong, N., Sarndhong, K., Islam, Md. A., and Sakunkoo, P.: An update on adverse health effects from exposure to PM2.5, Environmental Advances, 18, 100603, https://doi.org/10.1016/j.envadv.2024.100603, 2024.

Saurette, D. D., Heck, R. J., Gillespie, A. W., Berg, A. A., and Biswas, A.: Divergence metrics for determining optimal training sample size in digital soil mapping, Geoderma, 436, 116553, https://doi.org/10.1016/j.geoderma.2023.116553, 2023.

Shah, V., Jacob, D. J., Li, K., Silvern, R. F., Zhai, S., Liu, M., Lin, J., and Zhang, Q.: Effect of changing NO_{<i>x</i>} lifetime on the seasonality and long-term trends of satellite-observed tropospheric NO₂ columns over China, Atmos. Chem. Phys., 20, 1483–1495, https://doi.org/10.5194/acp-20-1483-2020, 2020.

Sharma, S., Chandra, M., and Kota, S. H.: Health Effects Associated with PM2.5: a Systematic Review, Curr Pollution Rep, 6, 345–367, https://doi.org/10.1007/s40726-020-00155-3, 2020.

Shetty, S., Schneider, P., Stebel, K., David Hamer, P., Kylling, A., and Koren Berntsen, T.: Estimating surface NO2 concentrations over Europe using Sentinel-5P TROPOMI observations and Machine Learning, Remote Sensing of Environment, 312, 114321, https://doi.org/10.1016/j.rse.2024.114321, 2024.

Sillman, S.: The relation between ozone, NOx and hydrocarbons in urban and polluted rural environments, Atmospheric Environment, 33, 1821–1845, https://doi.org/10.1016/S1352-2310(98)00345-8, 1999.

Steinbacher, M., Zellweger, C., Schwarzenbach, B., Bugmann, S., Buchmann, B., Ordóñez, C., Prevot, A. S. H., and Hueglin, C.: Nitrogen oxide measurements at rural sites in Switzerland: Bias of conventional measurement techniques, J. Geophys. Res., 112, 2006JD007971, https://doi.org/10.1029/2006JD007971, 2007.

Suleiman, R.: TEMPO gridded NO2 tropospheric and stratospheric columns V03 (PROVISIONAL), https://doi.org/10.5067/IS-40E/TEMPO/NO2_L3.003, 2024.

Thangavel, P., Park, D., and Lee, Y.-C.: Recent Insights into Particulate Matter (PM2.5)-Mediated Toxicity in Humans: An Overview, IJERPH, 19, 7511, https://doi.org/10.3390/ijerph19127511, 2022.

Thiagarajan, P. and Ghosh, S.: Jensen–Shannon divergence based novel loss functions for Bayesian neural networks, Neurocomputing, 618, 129115, https://doi.org/10.1016/j.neucom.2024.129115, 2024.

Toledo, A. S. O., Silini, R., Carpi, L. C., and Masoller, C.: Outlier mining in high-dimensional data using the Jensen–Shannon divergence and graph structure analysis, J. Phys. Complex., 3, 045011, https://doi.org/10.1088/2632-072X/aca94a, 2022.

Tsigalou, C., Panopoulou, M., Papadopoulos, C., Karvelas, A., Tsairidis, D., and Anagnostopoulos, K.: Estimation of low-density lipoprotein cholesterol by machine learning methods, Clinica Chimica Acta, 517, 108–116, https://doi.org/10.1016/j.cca.2021.02.020, 2021.

Urbanowicz, T., Skotak, K., Filipiak, K. J., Olasińska-Wiśniewska, A., Szczepański, K., Wyrwa, M., Sikora, J., Tykarski, A., and Jemielity, M.: Long-Term Exposure of Nitrogen Oxides Air Pollution (NO2) Impact for Coronary Artery Lesion Progression—Pilot Study, JPM, 13, 1376, https://doi.org/10.3390/jpm13091376, 2023.

2021 TIGER/Line® Shapefiles: https://www.census.gov/cgi-bin/geo/shapefiles/index.php?year=2021&layergroup=Roads, last access: 21 February 2025.

U.S. 2020 Urban Areas Shapefile: https://www2.census.gov/geo/tiger/TIGER_RD18/LAYER/UAC20/, last access: 21 February 2025.

Van Der A, R. J., Eskes, H. J., Boersma, K. F., Van Noije, T. P. C., Van Roozendael, M., De Smedt, I., Peters, D. H. M. U., and Meijer, E. W.: Trends, seasonal variability and dominant NO_x source derived from a ten year record of NO_2 measured from space, J. Geophys. Res., 113, 2007JD009021, https://doi.org/10.1029/2007JD009021, 2008.

Van Geffen, J., Boersma, K. F., Eskes, H., Sneep, M., Ter Linden, M., Zara, M., and Veefkind, J. P.: S5P TROPOMI NO₂ slant column retrieval: method, stability, uncertainties and comparisons with OMI, Atmos. Meas. Tech., 13, 1315–1335, https://doi.org/10.5194/amt-13-1315-2020, 2020.

Veefkind, J. P., Aben, I., McMullan, K., Förster, H., De Vries, J., Otter, G., Claas, J., Eskes, H. J., De Haan, J. F., Kleipool, Q., Van Weele, M., Hasekamp, O., Hoogeveen, R., Landgraf, J., Snel,

R., Tol, P., Ingmann, P., Voors, R., Kruizinga, B., Vink, R., Visser, H., and Levelt, P. F.: TROPOMI on the ESA Sentinel-5 Precursor: A GMES mission for global observations of the atmospheric composition for climate, air quality and ozone layer applications, Remote Sensing of Environment, 120, 70–83, https://doi.org/10.1016/j.rse.2011.09.027, 2012.

Venkatram, A.: Applications of Pollutant Frequency Distributions, Journal of the Air Pollution Control Association, 29, 251–253, https://doi.org/10.1080/00022470.1979.10470788, 1979.

Virta, H., Ialongo, I., Szeląg, M., and Eskes, H.: Estimating surface-level nitrogen dioxide concentrations from Sentinel-5P/TROPOMI observations in Finland, Atmospheric Environment, 312, 119989, https://doi.org/10.1016/j.atmosenv.2023.119989, 2023.

Wang, F. and Zhang, Z.: Correlation Structure and Co-Movement of Hunan Province's Air Pollution: Evidence from the Multiscale Temporal Networks, Atmosphere, 14, 55, https://doi.org/10.3390/atmos14010055, 2022.

Wang, Y., Bechle, M. J., Kim, S.-Y., Adams, P. J., Pandis, S. N., Pope, C. A., Robinson, A. L., Sheppard, L., Szpiro, A. A., and Marshall, J. D.: Spatial decomposition analysis of NO2 and PM2.5 air pollution in the United States, Atmospheric Environment, 241, 117470, https://doi.org/10.1016/j.atmosenv.2020.117470, 2020.

Xia, X., Meng, X., Liu, C., Guo, Y., Li, X., Niu, Y., Lam, K. B. H., Wright, N., Kartsonaki, C., Chen, Y., Yang, L., Du, H., Yu, C., Sun, D., Lv, J., Chen, J., Yang, X., Gao, R., Wu, S., Kan, H., Chan, K. H., Li, L., Chen, Z., Chen, J., Chen, Z., Clarke, R., Collins, R., Li, L., Lv, J., Peto, R., Walters, R., EdrisMohamed, A., Pozarickij, A., Iona, A., Wang, B., Clarke, C., Kartsonaki, C., Schmidt, D., Avery, D., Bennett, D., Fry, H., Du, H., Lam, H., Turnbull, I., Millwood, I., Liu, J., Clarke, J., Chan, K. H., Kolhe, K., Lin, K., Wang, L., Yang, L., Kakkoura, M., Rahmati, M., Barnard, M., Mazidi, M., Wright, N., Yao, P., Ryder, P., Im, P. K., Harish, P., Nie, Q., Stevens, R., Clarke, R., Walters, R., Boxall, R., Morris, S., Gilbert, S., Yang, X., Chen, Y., Chen, Z., Han, X., Hou, C., Xia, Q., Liu, C., Lv, J., Pei, P., Sun, D., Yu, C., Pan, L., Pang, Z., Gao, R., Li, S., Duan, H., Wang, S., Liu, Y., Du, R., Zang, Y., Cheng, L., Tian, X., Zhang, H., Zhai, Y., Ning, F., Sun, X., Li, F., Lv, S., Wang, J., Hou, W., Sun, W., et al.: Associations of long-term nitrogen dioxide exposure with a wide spectrum of diseases: a prospective cohort study of 0·5 million Chinese

adults, The Lancet Public Health, 9, e1047–e1058, https://doi.org/10.1016/S2468-2667(24)00264-0, 2024.

Xu, A. and Xiang, C.: Assessment of the Emission Characteristics of Major States in the United States using Satellite Observations of CO2, CO, and NO2, Atmosphere, 15, 11, https://doi.org/10.3390/atmos15010011, 2023.

Yan, J., Li, P., Gao, R., Li, Y., and Chen, L.: Identifying Critical States of Complex Diseases by Single-Sample Jensen-Shannon Divergence, Front. Oncol., 11, 684781, https://doi.org/10.3389/fonc.2021.684781, 2021.

Yu, Z. and Li, X.: The Temporal–Spatial Characteristics of Column NO2 Concentration and Influence Factors in Xinjiang of Northwestern Arid Region in China, Atmosphere, 13, 1533, https://doi.org/10.3390/atmos13101533, 2022.

Zhang, R., Wang, Y., Smeltzer, C., Qu, H., Koshak, W., and Boersma, K. F.: Reconciling the differences between OMI-based and EPA AQS in situ NO₂ trends, https://doi.org/10.5194/amt-2017-410, 25 January 2018.

Zhao, D., Yan, W., You, M., Zhang, J., Arun, P. V., Jiao, C., Wang, Q., and Zhou, H.: Hyperspectral Anomaly Detection Based on Empirical Mode Decomposition and Local Weighted Contrast, IEEE Sensors J., 24, 33847–33861, https://doi.org/10.1109/JSEN.2024.3455258, 2024.

Zoogman, P., Liu, X., Suleiman, R. M., Pennington, W. F., Flittner, D. E., Al-Saadi, J. A., Hilton, B. B., Nicks, D. K., Newchurch, M. J., Carr, J. L., Janz, S. J., Andraschko, M. R., Arola, A., Baker, B. D., Canova, B. P., Chan Miller, C., Cohen, R. C., Davis, J. E., Dussault, M. E., Edwards, D. P., Fishman, J., Ghulam, A., González Abad, G., Grutter, M., Herman, J. R., Houck, J., Jacob, D. J., Joiner, J., Kerridge, B. J., Kim, J., Krotkov, N. A., Lamsal, L., Li, C., Lindfors, A., Martin, R. V., McElroy, C. T., McLinden, C., Natraj, V., Neil, D. O., Nowlan, C. R., O′Sullivan, E. J., Palmer, P. I., Pierce, R. B., Pippin, M. R., Saiz-Lopez, A., Spurr, R. J. D., Szykman, J. J., Torres, O., Veefkind, J. P., Veihelmann, B., Wang, H., Wang, J., and Chance, K.: Tropospheric emissions: Monitoring of pollution (TEMPO), Journal of Quantitative Spectroscopy and Radiative Transfer, 186, 17–39, https://doi.org/10.1016/j.jqsrt.2016.05.008, 2017.